Particle-in-Cell Charged-Particle Simulations, Plus Monte Carlo Collisions With Neutral Atoms, PIC–MCC

C. K. Birdsall, *Life Fellow, IEEE*

(Invited Paper)

Abstract— **Many-particle (meaning 1000's) charged-particle plasma simulations using spatial meshes for the electromagnetic field solutions, particle-in-cell (PIC) merged with Monte Carlo collision (MCC) calculations, are coming into wide use for application to partially ionized gases. This paper emphasizes the development of PIC computer experiments since the 1950's starting with one-dimensional (1-D) charged-sheet models, the addition of the mesh, and fast direct Poisson equation solvers for 2-D and 3-D. The finite-size particle-in-mesh (finite Δx, Δt) theory of Langdon [51]–[53] is presented in part to display the effects of too small $\lambda_D/\Delta x$, even for Maxwellian velocity distributions, as a caution, for example, when some ions are cooled to background gas temperatures by charge exchange. Early work on adding collisions to 1-D charge-sheet models by Burger [28] and Shanny *et al.*[76] are presented, with many of the elements of current Monte Carlo codes. Bounded plasma modeling is presented with electrode charges and external R, L, C, and $V(t)$, $I(t)$ sources now in use on fast desktop computers as real-time computer experiments, complementing analytic modeling and laboratory experiments. The addition of Monte Carlo collisions (usually done with irregular timesteps) to PIC (usually done with uniform Δt's) is displayed as a developing art, relying on experimental total cross sections and approximate analytical differential cross sections to produce changes in charged-particle speed and direction due to collisions with neutrals, so far including elastic, excitation, ionization, charge exchange, and attachment processes.**

I. Introduction

THE plasma medium, consisting of electrons, ions, neutral atoms and molecules, and particles, is very complicated to understand. Theory and modeling provide guide-lines for design of devices; experiments provide a variety of measurements. Simulations provide insight, and numbers, computer experiments. Interactions among this trio have proven effective and efficient in advancing plasma science and engineering.

This report leads the reader through the development over the past four decades of many-particle particle-in-cell (PIC) simulations and into including charged-particle collisions with neutral atoms using Monte Carlo methods. Some mention will be made of doing Coulomb collisions using PIC codes. We then provide some details of adding the collisions between the charged particles and neutral atoms. The result is many-particle simulations with many of the features met in low-temperature collisional plasmas; for example, with applications to plasma-assisted materials processing, but also related to warmer plasmas at the edges of magnetized fusion plasmas.

Collisionless many-particle plasma simulation is rich in history and may rate as one of the success stories in physics and engineering using the modern digital computer, along with such advances as numerical wind tunnels and space craft control and communications—both complementing theory and experiment and, in some cases, being the main ingredient. This richness extends also to the breadth of methods, making it difficult to mention here all the bits and pieces practitioners like to have at their fingertips.

This review has the following organization. Section II covers early one-dimensional sheet models, roughly from the 1950's to mid 1960's. Section III covers early two- and three-dimensional models with mathematical grids (meshes), labeled particle-in-cell (PIC) or cloud-in-cell (CIC), from about the mid 1960's onwards. Section IV covers the theory of simulation with particle-shape factors and so on, from about 1970 onwards. Section V covers early work on electron-neutral elastic collisions. Section VI covers early work on electron–ion Coulomb collisions. Section VII covers more early Coulomb collision work. Section VIII covers the bounded models that we and others have developed for studying plasma sheaths and edges. Section IX introduces the detailed treatment of several kinds of collision processes between the charged particles and neutral gas atoms.

Several books on plasma and many-particle simulations are referred to frequently. They appear in the references as Birdsall and Bridges [7], Dunn [37], Hockney and Eastwood [50], Birdsall and Langdon [12], Tajima [82]. There are three review books (vols. 9 and 16 of *Methods of Computational Physics*, Alder *et al.*, Eds., 1970 and 1976, respectively, and *Multiple Time Scales*, Brackbill and Cohen, Eds., 1985). An excellent general coverage is Potter's 1973 book [70], covering PIC methods in fluids as well as with particles.

There are also numerous introductory or review articles or chapters: For example, Buneman and Dunn [23], Birdsall and Dawson [11], Denavit and Kruer [36], and Dawson [34].

Lastly, there are the *Proceedings* (several page articles) of the Conferences on Numerical Simulations of Plasmas, begun in 1967, up to the 14th Annual Conference in 1990.

A word on the general temperament of the field of many charged-particle simulations. It is quite remarkable that charged-particle simulations have remained very close to the *use of first principles*, meaning the use of classical mechanics for the equations of motion ($\boldsymbol{f} = m\boldsymbol{a} = q\ (\boldsymbol{E} + v \times \boldsymbol{B})$ and using Maxwell's equations for the $(\boldsymbol{E}, \boldsymbol{B})$ fields generated by the particle densities $(\rho, \boldsymbol{J})$. Very little *ad hoc* or approximate physics has crept in. Users have gained considerable confidence in their

Manuscript received August 6, 1990; revised November 30, 1990. This work was supported by the U.S. Department of Energy, Office of Fusion Energy, Applied Plasma Physics under Contract No. FD-DE-FG03-90ER54079, and the Office of Naval Research under Contract No. FD-N00014-90-J-1198. Some of this work began with support from Varian, through Dr. J. Helmer, with a California MICRO matching grant.

The author is with the Plasma Theory and Simulation Group, Department of Electrical Engineering and Computer Sciences, University of California, Berkeley, Berkeley, CA 94720.

IEEE Log Number 9042658.

results, warranted by applying various cross checks. The recent entry into adding (charged-particle) + (gas-particle) + (surface-particle) reactions together relies on the use of probabilities of many reactions, not all known well. The science of particle chasing with superparticle electrons and ions is on relatively firm ground; that of superparticle collisions, including neutrals, satisfactorily mimicking many elementary particle collisions, concerns us.

And yet a last word on applications. For a long time, simulations were employed primarily to provide the *essence* of plasma behavior, simply because there was little recourse except to simulations in order to obtain the nonlinear, inhomogeneous, and anisotropic plasma behavior. In this period the use was relatively sophisticated, done by a select few, and was performed on mainframe computers in batch mode (with a great deal of patience and persistence). However, simulations are presently being employed to provide *complete details* of plasma behavior (whole devices, machines, with external connections) in *user friendly, high interactive, real time computer experiments.* Even the numerics (such as Δx, Δt, superparticles, etc.) are becoming hidden from sight so that the physics (and chemistry) can be made foremost. The sequence evolving roughly models with one-dimensional displacements (1-D), with three velocity components ($3v$) on fast PC's (perhaps up to 10^4 particles), moving to 2-D$3v$ on fast workstations (perhaps up to 10^5 particles), to 3-D$3v$ on supercomputers (with 10^6 or more particles), and finally on to massively parallel computation. We cannot emphasize too strongly the importance to the general or even casual user of this evolution. The evolution (or revolution) is fueled, as always, by the continued increase in speed and memory of computers and by attention to graphics and visualization.

There is a long way yet to go. Real time fast PC runs using Δt's of, say, nanoseconds, now process 5000 particles per real second at best; this speed means run times (say, for 5000 particles running 10^5 time steps) of 30 h. This run time drops to 3 h on a fast workstation, and a few minutes on a supercomputer. The run time on these machines goes up, as we switch to 2-D and 3-D and add many more cells and particles. The bottom line here is the belief that the 1-D$3v$ (PC), and 2-D$3v$ (WS, SC) use of many-particle simulations by modelers, designers, and operators of machines (as in plasma processing) is now sufficiently fast and friendly, with meaningful physics (and soon chemistry) output so that interactive computer experiments can greatly aid and complement laboratory experiments and manufacturing on a daily basis.

II. Early One-Dimensional Many-Particle Simulations

Old timers in a field are often questioned why this or that model was not used—answering, many times, that such models *were* used. Our habits of searching the literature are imperfect, occasionally lazy, and not helped by computer databases going back only 10 or 15 years. My object in this section is to display and discuss early 1-D models, which still could be used today, but, by and large, are not.

Early on it was determined that useful charged-particle simulations could be done with a small number of particles, many orders of magnitude fewer than in a real plasma. Obviously, there needs to be a reasonable number of computer particles (also called superparticles) distributed across the shortest spatial feature of interest (shortest wavelength or closest electrodes, walls). There needs to be a sufficient number to overcome the increased graininess (shot noise, $1/\sqrt{N}$ noise, etc.) of a small number of particles (say, 10 000) representing a much larger number in the laboratory (say, $n = 10^{18}/\mathrm{m}^3$ over a cube 0.1 m on a side, or 10^{15}). An easy check on the choice of number needed is simply to run with twice as many computer particles and see whether the simulation reproduces the same physics. Another check, very essential, is to compare simulation results with analytic or numerical predictions (from kinetic or fluid models); we are happy to note that many such intended checks have actually led to improvements in the predictions, as the computer model usually has fewer assumptions.

Let us look at the simplest models, such as were used in the 1950's on the (then) emerging fast digital computers. These were:

- one-dimensional (charge acceleration, velocity, and displacement in x only)
- electrostatic (E_x (x) from Gauss's Law or $\phi(x)$ from Poisson's equation)
- collisionless (to be explained)
- sheet or disk particles (zero thickness)
- no mathematical grid

and probably no graphical output (all numbers).

There was some particle modeling in the 1940's. Here is a short summary (from [50, p. 362]):

> Techniques for vacuum tubes were pioneered during World War II by Professor D. R. Hartree when he headed the Manchester University Group for the Committee on Valve Development (CVD) of the British Admiralty. Around 1943 Professor Hartree and Phyllis Nicolson (1941–1944) computed by hand on a desk calculator the orbits of about 30 interacting electrons in a magnetron using a one-dimensional approximation for the electron field (see Buneman and Dunn [23, p. 36]. Their model included the effect of space charge and the electric and magnetic fields, but because of its restriction to one-dimension was not able to represent fully the two-dimensional charge flow in a magnetron. Later, Hartree [45] made a study of electron flow in a one-dimensional diode in a similar way, and observed the initial transient that occurs as an empty diode fills with electrons.

Fig. 1 shows the electric field of one electron sheet in a short circuited diode. The sheet has charge density $\rho_s(\mathrm{C}/\mathrm{m}^2)$, mass density $m_s(\mathrm{kg}/\mathrm{m}^2)$, with $\rho_s/m_s = q/m$ of the computer particle. The fields are obtained by applying Gauss's law, producing the sheet acceleration as:

$$m_s \ddot{x}_1 = -\frac{\rho_s^2}{\varepsilon_0}\left(\frac{1}{2} - \frac{x_1}{d}\right). \tag{1}$$

This one-sheet model motion may be solved analytically for many approximate answers (see [7, chap. 3]). We move on to the multiple sheet model shown in Fig. 2. The average field at sheet j is now given by adding in the fields of all of the sheets, given by:

$$\overline{E}(x_j) = \frac{\rho_s}{\varepsilon_0}\left[\sum_{i=1}^{M}\left(\frac{x_i}{d}\right) - j + \frac{1}{2}\right] \tag{2}$$

to which an applied field may be added. We solve simultaneously the set of equations of motion, one for each sheet using the known fields. This solution is done numerically, using finite-difference approximations to dv/dt and dx/dt, each time centered and integrated using a time step Δt which is small compared with the shortest period expected (e.g., $\omega_{\max}\Delta t \leq 2\pi/30$). The solution produces new velocities and new positions; the latter produce new fields, allowing the next time step to be taken, as shown in

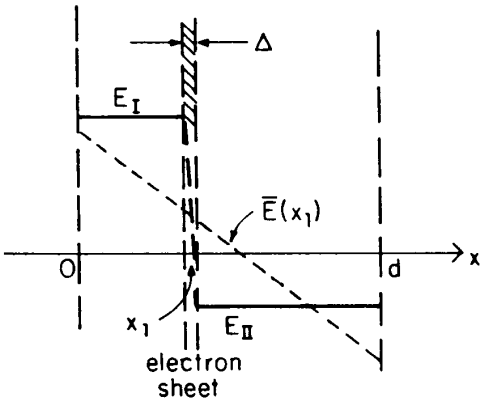

Fig. 1. Electric field produced by a sheet charge at position x_1 between short-circuited electrodes. The quantity $\overline{E}$ is the average field $\frac{1}{2}(E_{\mathrm{I}} + E_{\mathrm{II}})$, shown as a function of the charge position x_1 (from Birdsall and Bridges [7]).

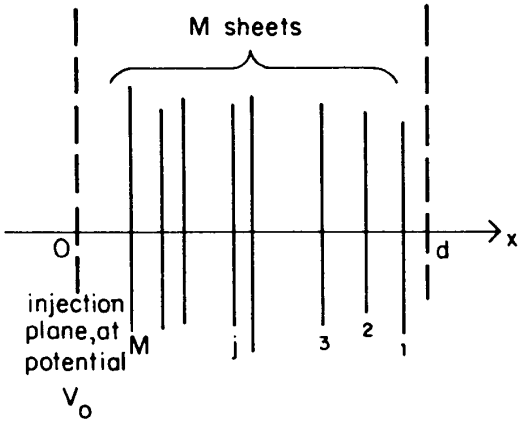

Fig. 2. Ordering of sheets within the interelectrode space (from Birdsall and Bridges [7]).

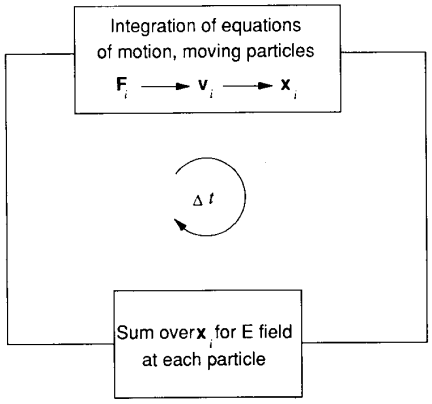

Fig. 3. Computing sequence for electric fields obtained directly from particle positions, via Gauss's Law.

Fig. 3. The entire simulation run might be 1000 Δt steps long, at say, 30 cycles of the highest frequency. Note that it is possible for an electron sheet to pass another during a time step, changing the field (force) on the sheets involved within Δt, an error. The effect of exceeding a limiting current, producing virtual cathode oscillations, was observed from this model [60], [6] (currently called "vircator" devices).

Moving closer to warm particle behavior, let the 1-D diode represent an electron gun to be used in an electron beam device. The left-hand electrode is a hot cathode, thermionically emitting electrons uniformly (but randomly) in time, with a (half) Maxwellian velocity distribution (at the temperature of the electrode). The right-hand electrode is the anode, held at a voltage positive with respect to the cathode by an external battery. The time-independent analytic solution for this model was given by Fry [43] and Langmuir [57], improving on the cold solution by Child [30]. The time-dependent model was tackled by many workers in the 1950's, seeking the fluctuations in current (relative to full shot-noise) and velocity to use as input conditions for microwave beam tubes. Hockney and Eastwood [50] pay tribute to a milestone paper as follows:

At about the time the first digital computers became available, and perhaps the earliest simulation on such computers, was the study of noise in a high-frequency diode by Tien and Moshman [85] of Bell Laboratories. They used a Univac I to simulate a one-dimensional diode with about 360 electrons sheets and a physical time step of 2 ps. About 3000 time steps were taken, each of which required between 25 and 40 s of computer time. The total computing task must rank as one of the most impressive achievements of early device modeling, requiring as it did some 25 h of reliable computing on a first generation vacuum-tube computer with a mercury delay-line store of only about 1000 numbers.

The model simulated by Tien and Moshman [85] had emission statistics (time and velocity of emission derived from weighted random-number-generating routines, Monte Carlo technique) with motion and fields solved for as described earlier in this section. The well-known space-charge smoothing of shot noise at low frequencies was observed, along with a dip and peak near $\omega = \omega_p$ at the potential minimum, not known earlier, and perhaps open to question. This simulation is, in some minds, the first warm species simulation; indeed, there was a plasma-like electron Debye cloud next to the cathode, with plasma-like potential fluctuations (near the plasma frequency). The authors initiated several modeling and diagnostic techniques still in use today. For example, for determining the velocities we still equate the normalized cumulative velocity distribution (up to the v to be injected) to a uniform set of numbers, sometimes random.

The next step was to use two species, electrons and ions, with very nearly equal number density, nearly electrically neutral, as in a plasma. However, the initial plasma models were intended for obtaining collective behavior in uniform plasmas; that is, propagating as $\exp j(\omega t - kx)$, with real k but complex ω, allowing for growth and decay in time. As such, it was allowable to use *periodic models* of length L, with particles passing beyond $x = 0$, L reinserted at the other end. The plasma region studied is like a portion of an infinite plasma, but with wavenumbers $kL = 2\pi, 4\pi, 6\pi$, etc.; i.e., wavelengths submultiples of L. The simulation field solutions are again readily obtained, taking advantage of the facts that the periodicity of $E_x(x)$ used in $\nabla \cdot \boldsymbol{E} = \rho/\varepsilon_0$ integrated over L demands $\int \rho\, dx = 0$, no

net charge, overall neutrality; the periodicity of $\phi(x)$ used in $-\nabla\phi = \boldsymbol{E}$ integrated over L demands $\int E_x\,dx = 0$, no net (or average) field. Hence to obtain E, start at $x = 0$ with $E(x = 0)$ set to E_0, then sum:

$$E_0 x_1 + \left(E_0 + \left(\frac{\rho_s}{\varepsilon_0}\right)_1\right)(x_2 - x_1) + \left(E_0 + \left(\frac{\rho_s}{\varepsilon_0}\right)_1 + \left(\frac{\rho_s}{\varepsilon_0}\right)_2\right) \cdot (x_3 - x_2) + \text{etc.},$$

across to $x = L$; set the sum to zero to obtain:

$$E_0 L = \sum_{i=1}^{N} \left(\frac{\rho_s}{\varepsilon_0}\right)_i x_i. \tag{3}$$

Having found E_0, the mean field at the jth sheet is:

$$\overline{E}_j = E_0 + \frac{1}{2}\sum_{i=1}^{j}\left(\frac{\rho_s}{\varepsilon_0}\right)_i \tag{4}$$

to be used in:

$$(m_s)_j \ddot{x}_j = \rho_{s,j}\overline{E}_j. \tag{5}$$

Again, integrate all the equations of motion simultaneously over Δt as before (Fig. 3) and repeat for as many Δt as needed.

One of the first to use this model was Buneman at Stanford [20]. We now quote again from [50, pp. 362–363]:

> Another early one-dimensional model was developed at Stanford University by Buneman [20], who himself has been a student of Hartree and had worked in the Manchester CVD group. This model with 512 sheets was programmed by D. Thoe of Lockheed on a Univac 1103AF, and used to demonstrate the unexpectedly rapid dissipation of currents when entering ionized media.

He followed cold electrons drifting through cold ions (overall neutral and collisionless), which is physically unstable at long wavelengths. The dispersion relation from linearized fluid modeling, with wave behavior as exp $j(\omega t - kx)$, is:

$$\varepsilon_{\text{longitudinal}} = \varepsilon_0\left(1 - \frac{\omega^2_{p,\text{ions}}}{\omega^2} - \frac{\omega^2_{p,\text{electrons}}}{(\omega - kv_0)^2}\right) = 0 \tag{6}$$

where v_0 is the electron drift speed. Using $n_{i0} = n_{e0}$ means that:

$$\omega_{p,\text{electrons}}/\omega_{p,\text{ions}} = \sqrt{m_i/m_e} \gg 1 \tag{7}$$

the so-called strong-beam model. (In his model, $m_i/m_e = 1836$.) The growth rate $\omega_{\text{imaginary}}$ on the order of $\omega_{p,\text{ions}}$ is observed to hold from small initial perturbations up to where the instability becomes nonlinear and then saturates, defined as when the conversion of the beam kinetic energy to electrostatic energy reaches a peak. The remarkable result is that the electron beam becomes so scrambled by the instability that it loses its drift motion—indeed, has some electrons reflected, almost as if short-range momentum transfer collisions had occurred (but were not purposely included). Buneman observed that these collective effects amounted to an effective collision rate which was on the order of the growth rate, being rather large; that is:

$$\nu_{\text{effective}} \approx \omega_{\text{imaginary}} \approx \omega_{p_{\text{ions}}}. \tag{8}$$

This mechanism is one of several candidates for explaining "electron cooling" ($J \cdot E$ of electrons negative in the bulk plasma) in low-pressure RF discharges; the initially cool ions are heated.

The next big step with two species followed soon after, with simulations of warm (Maxwellian) electrons in a uniform immobile ion background. The initial article was by Dawson [33] and is considered by many to be *the plasma simulation milestone.* This was followed closely by complementary work by Eldridge and Feix [39], [40]. This model and accompanying kinetic theory truly opened the field, as Dawson showed that much of the theoretical kinetic behavior of collisionless plasmas could be observed in simulations with only 5 to 20 sheets in a Debye length, $N_D = n\lambda_D \approx 5$ to 20. This demonstration was indeed a revelation to most plasma physicists, accustomed to a 3-D world with:

$$N_D = n\lambda_D^3 \approx 10^4 - 10^9.$$

The fields for electron sheets imbedded in a uniform ion background, still periodic, are particularly simple. Each electron has an equilibrium position x_{j0} (no force felt), about which it performs simple harmonic motion at the plasma frequency:

$$(\ddot{x}_j - x_{j0}) = -\omega_p^2(x_j - x_{j0}). \tag{9}$$

Each electron may be independently excited. When these particles cross, they simply exchange equilibrium positions.

Dawson and Smith also used a model of two warm mobile species to investigate instabilities due to current [35], where the mean ion velocity was separated from the mean electron velocity (not dissimilar from Buneman's cold streaming). In their sheet model, using the fact that the force is constant between sheets with x, t orbits parabolic, they solved for the crossing times and then used the shortest time to advance the system (i.e., no crossing errors). His results confirmed theoretical conjecture about anomalous resistance for plasmas carrying large currents five years before such an effect was demonstrated convincingly in laboratory experiments. Dawson also used a crossing-error correction, as now when unlike species cross in a nearly neutral plasma the force change is more exaggerated than with one species only.

We leave the development of 1-D plasmas here. Numerous additions to modeling could be noted, such as: Addition of transverse velocity components; addition of a transverse static magnetic field; and magnetostatic models using current sheets rather than charge sheets. Of course, there were by now a long list of applications.

In all of the 1-D world with sheets, very little, if any, was done on the *theory* of simulation; that is, to display the effects of discrete particles, finite time steps and so on; it became necessary in the extensions to more dimensions, as we will observe.

III. Early Two- and Three-Dimensional Many-Particle Simulations

One-dimensional sheet models using Gauss's Law, Coulomb's Law, Ampere's Law, appropriate Green's functions, etc., are not readily extended to higher dimensions. Also, 3-D *particle-particle methods,* obtaining electric forces from vector sums of q_i/r_{ij}^2, have been used, but are not attractive for most models and have excessive costs (see [50, p. 19]). And then there is also the need for fully electromagnetic models. What to do?

The simulation community could have remained mostly in one-dimensionland and with various straightforward extensions. For example, 1-D can mean 1-D planar or 1-D cylindrical or 1-D spherical, where the charges are sheets, cylindrical, and spherical shells, respectively. Also, accounting for additional velocity components is readily done, (v_x, v_y, v_z) or (v_r, v_θ, v_z) or (v_r, v_θ, v_ϕ), respectively. Indeed, these 1-D3v models were developed in the

1960's (sometimes called $1\frac{1}{2}$-D models) for electrostatic, magnetostatic, and electromagnetic models, bounded and periodic. See, for example, Auer *et al.* [4], [5], Hasegawa and Birdsall [46], Langdon and Dawson [54], and Chen and Birdsall [29]. Such models are still widely used, imaginatively extended and stretched (as for collisions with neutrals, to be introduced later in this paper), now running readily on desktop computers, and still adding new knowledge. Obviously, if a first step on a complex plasma model can be done in 1-D3v, then do it!

One big step taken was the introduction of a *mathematical grid* (or *mesh*, Δx by Δy by Δz) overlaying all of the particles, to which charges were *assigned* (also called *weighted*) in order to create charge and current densities $(\rho, \boldsymbol{J})$ at the grid points. (See Fig. 4.) These densities were then used as source terms in solving Maxwell's equations for the fields $(\boldsymbol{E}, \boldsymbol{B})$ on the grid, to be re-assigned (weighted) as forces at the particles. Then the particles are moved in 1- or 2- or 3-D by integrating:

$$m\frac{d\boldsymbol{v}}{dt} = q(\boldsymbol{E} + \boldsymbol{v} \times \boldsymbol{B}), \qquad \frac{d\boldsymbol{v}}{dt} = \boldsymbol{x}. \tag{10}$$

The sequence is given in Fig. 5, adding weighting. It looks simple. Of course, grids were already long in use in fluid simulations, such that a variety of numerical methods were known. Birdsall and Langdon [12, p. 156] write:

> The plasma models we discussed originated at Stanford University in 1963. In order to make simulations in *two dimensions* economically practical, Buneman (in Yu *et al.* [91]) and Hockney [48], [49] developed a model which uses a *spatial grid* in which the charge density is found from the particle positions, Poisson's equation is solved in finite-difference form, and then the particle forces are interpolated from the grid. This is *much more efficient* than summing N^2 Coulomb interactions among N particles. They also realized that computational and physical problems associated with the divergent character of Coulomb field are eliminated; the interactions at small separations are smoothed, reducing the large-angle binary collisions which are of little interest in hot plasmas and which have been exaggerated in simulation because of the small number of particles used (Hockney [49]). Although simulation in one dimension was possible by other means, the new model offered simplicity and speed there, too (Dunn and Ho [37]; Berger *et al.* [27]; Buneman and Dunn [23]). Part of the gain was in the method of integrating the system forward in time. The algorithms were fast and preserved certain physical properties (Buneman [21]). The advantages of the grid approach were not immediately recognized elsewhere and much simulation was done for which the gridded model would have been more efficient.

Other people then developed versions of the gridded model with more accurate interpolation and different methods of solving Poisson's equation (Birdsall *et al.* [9]; Birdsall and Fuss [8], [10]; Morse and Nielson [63], [64]; Boris and Roberts [17]; Alder *et al.* [2]). Capping these efforts were the large-scale simulations done at Los Alamos Scientific Laboratory of several problems in the controlled thermonuclear fusion research program in 1968. Since then, simulation by these methods has been widely accepted as a plasma research tool.

We are less interested in the accuracy of individual particle orbits and more in the accuracy of *collective plasma phenomena.* Therefore, our analytical approach, terminology, and criteria are more that of the plasma physicist than of the numerical analyst studying, say, an initial-value problem for a small system of differential equations with no particular application in mind. In several places the collective properties of warm plasmas play a crucial role.

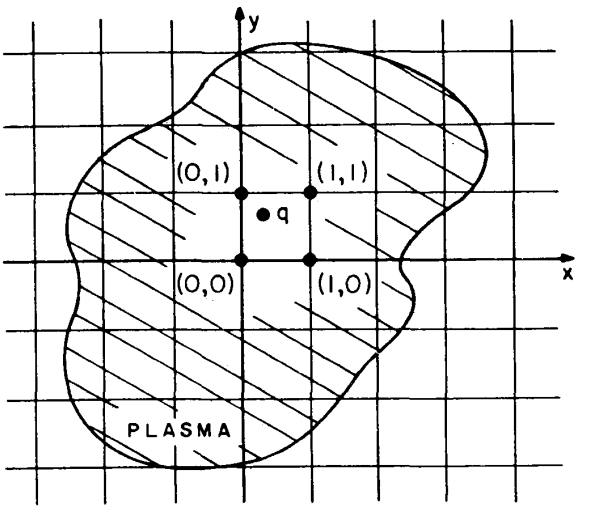

Fig. 4. A mathematical grid is set into the plasma region in order to measure charge and current densities ρ, J; from these we will obtain the electric and magnetic fields $\boldsymbol{E}$, $\boldsymbol{B}$ on the grid. A charged particle q at (x,y) will typically be counted in terms of ρ at the nearby grid points (0,0), (1,0), (1,1), (0,1), and in terms of $\boldsymbol{J}$ at the faces between these points. The force on q will also be obtained from the fields at these nearby points (from Birdsall and Langdon [12]).

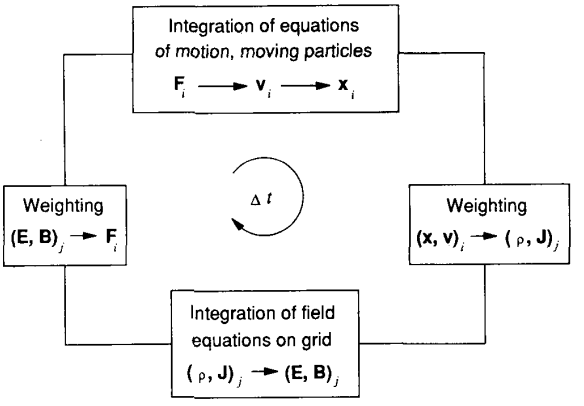

Fig. 5. Computing sequence for particle-mesh method; mover, weight particles to grid, field solve, weight fields to particle (from Birdsall and Langdon [12]).

The models obviously do *not* accurately reproduce the microscopic dynamics of a plasma. One must consider if and how such errors modify the macroscopic behavior. There are usually far too few particles. This causes discrete-particle effects such as exaggeration of fluctuations and collisions. There may also be too few particles for adequate representation in phase space of plasma phenomena such as the Landau damping wave-particle resonance. There can be serious problems with initial and boundary conditions. Round-off errors can usually be made negligible compared to other errors. Such sources of error are difficult to assess in practice. Some study of their nonphysical effects was needed. Much of this has been done through experiments with the models (Birdsall *et al.* [9]; Hockney [49];

Montgomery and Nielson [62]; Okuda [66], [67]).

In addition to empirical results, some theoretical analysis is desirable. This is true for the usual reasons that adding a good theory implies a better understanding than a stack of oscillograms or computer output alone. In Part Two we develop a theoretical understanding of errors caused by the finite-difference representation in space and time of the field equations and particle dynamics. One hopes the theory also predicts unexpected interesting results that can be verified experimentally; we describe some results which we think are in this category.

There has been some approximate discussion of the models. Smoothing and noise aspects of the spatial grid were recognized early (e.g., Hockney [49]; Birdsall and Fuss [8], [10]) and approximate theoretical descriptions made of each (Hockney [49]; Langdon and Birdsall [55]; Okuda and Birdsall [68]). The time integration was considered heuristically (Buneman [21]).

However, regarding the space-time grid simply as a source of smoothing and of noise fails to uncover some very important effects involving coherent interaction between the plasma and the sampling in space and time. Some theory has appeared which includes exactly the effects of the finite-differencing and is applied to linear wave dispersion and stability and to energy conservation (Lindman [59]; Langdon [52]). We have also looked at fluctuations and collisions (Langdon [53, chap. 12]). The theory is quite complete and in about as tidy a form as is possible for such a system. Different parts of the simulation algorithms are easily identified and changes made. Where possible, we keep the results in a form permitting easy comparison with real plasma theory.

Hockney and Eastwood [50, p. 363] say the following:

Burger, working as a student of Buneman, refined the one-dimensional model by using integer arithmetic and a mesh for the calculation of the fields. This model permitted the simulation of 10 000 electron sheets on an IBM 7090, and was used to study the operation of cesium thermionic converters and plasma diodes (Burger [25], [26]; Burger *et al.* [27]).

The extension of the simulations to two-dimensions was made possible about 1964 by a new Poisson-solver developed by Hockney [48] also working as a student of Buneman but on plasma simulation. This allowed the simulation of about 2000 rods of charge and was successfully used to demonstrate anomalous diffusion in plasma (Hockney [49]); the full two-dimensional charge flow in magnetrons (Yu *et al.* [91])—thus completing, some 20 years later, Hartree's work in the war; and the neutralization of ion-beams intended for spaceship propulsion (Wadhwa *et al.* [90]).

Burger [25, p. 45] says, " . . . coarse-graining in space was first used by Dunn and Ho [37] and it was also applied by Hockney for the computer model of a two-dimensional plasma [47]."

The initial particle-mesh work of Burger (1-D) and Hockney (2-D) used an obvious charge assignment, just counting the number of particles between grid points and assigning the corresponding density to the cell center, called, appropriately, *nearest-grid-point* (NGP). Similarly, all of the particles in a given cell were assigned the same force or field as at the cell center. The overall name *particle-in-cell* (PIC) is very appropriate. (The original PIC method for fluid dynamics was introduced by Harlow [44] for collision-dominated hydrodynamic modeling, who writes [44, p. 329]: " . . . linear interpolation among cellwise velocities of the four nearest cell centers to the particle position. This is equivalent to an areawise velocity weighting . . . linearly interpolated velocity weighting procedure . . . .") (Also see Potter [70, pp. 155–161].) The remarkable interpretation that has evolved is that the particles could now be viewed as having *finite size,* with a diameter roughly that of the cell, and being tenuous and cloud-like. Hence the name *cloud-in-cell* (CIC) is also appropriate. The NGP assignments, also known as *zero-order weighting,* gave a staircase-like approximation to the $1/r$ or $1/r^2$ force between two particles (2-D, 3-D) as one particle approached the other. Going to *first-order weighting* changes the force to piecewise linear in space; *second-order (spline) weighting* leads to piecewise parabolas, etc. But when two finite-size particles cross (i.e., are in the same cell), the interparticle force drops to zero and then changes direction as the particles separate. The zero, rather than infinite, force at crossing (as $r \rightarrow 0$) is a loss of resolution of the short-range force; hence a loss of short-range Coulomb collisions at impact parameters less than a cell diameter. If such collisions are to be included, then they have to be reinserted ("accelerated"), say, with particle–particle methods within a cell. The combined model is then a particle-mesh, particle–particle method, long range plus short range (well covered in [50, chap. 8]). This loss of short-range force may also be viewed as the *smoothing effect of the grid* and is desirable when primarily seeking long-range effects; indeed, the particle-mesh model is usually quite (short-range) "collisionless," a boon in those plasma simulations where the (wave) frequencies of interest are much larger than Coulomb collision frequencies. Indeed, most field solvers currently are so fast that the particle pusher (weighting, integrating) is the major time consumer in a time step.

The linear-weighting charge assignment (first-order spline) in 2-D is illustrated in Fig. 6, usually called *area weighting* for obvious reasons. Such PIC or CIC linear weights are probably the most commonly used. Note that the PIC and CIC assignments do not differ here, but that they do in cylindrical and spherical (and other) coordinate systems.

A second step was relating the particle and force weighting to the effective *finite-particle shape* (see historical note in [13]). Langdon especially developed considerable simulation theory involving the particle-shape factor $S(\boldsymbol{x})$ and its spatial Fourier transform $S(\boldsymbol{k})$, showing that much of the plasma theory known for point particles of charge q holds for finite-size particles by replacing q by $qS(k)$, such as replacing the plasma frequency ω_p by $\omega_p S(k)$. Langdon's theory (and that of others) appears in many articles and is presented in detail in the three books [50], [12], [82] recommended earlier. The simulation theory showed the effects of choices of numerical parameters Δx and Δt. As we have found close agreement between theory and simulations, we have gained considerable confidence in the simulations as truly representing physics.

A third step was the invention of fast 3-D particle integrators, from force to new velocity to new position, including both $\boldsymbol{E}$ and $v \times \boldsymbol{B}$, with contributions by Hockney [49], Buneman [21], and Boris [18]. These are variations on the *explicit leap-frog scheme:*

$$m\frac{d\boldsymbol{v}}{dt} = \boldsymbol{f} \rightarrow m\frac{\boldsymbol{v}^{t+1/2} - \boldsymbol{v}^{t-1/2}}{\Delta t} = f(\boldsymbol{x}^t, \boldsymbol{v}^t) \qquad (11)$$

$$\frac{d\boldsymbol{x}}{dt} = \boldsymbol{v} \rightarrow \frac{\boldsymbol{x}^{t+1} - \boldsymbol{x}^t}{\Delta t} = \boldsymbol{v}^{t+1/2}. \qquad (12)$$

Integration starts from known $\boldsymbol{x}^t$ and $\boldsymbol{x}^{t-1/2}$ (where $t - 1/2$

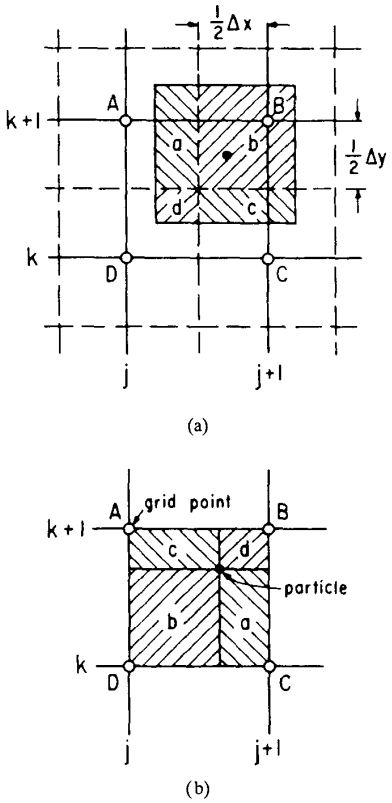

Fig. 6. Charge assignment for linear weighting in two dimensions. Areas are assigned to grid points; i.e., area a to grid point A, area b to B, etc., as if by NGP, with the particle center located as indicated. (a) The CIC cloud interpretation. (b) The PIC bilinear interpolation interpretation. (From Birdsall and Langdon [12].)

means $t - \Delta t/2$), and produces x and $v\,\Delta t$ later. These two first-order difference equations are time-centered, so that the integration of both together is second-order accurate (Δt^2 error term). This method is stable for simple harmonic motion (e.g., plasma oscillations) for $\omega_{\max}\Delta t < 2$, with good accuracy for $\omega_{\max}\Delta t \leq 0.2$.

Roughly ten years later (1980) a fourth step was the invention of *implicit particle and field integrators* by various workers (see [12, p. 205], [14]) which allowed $\omega_{\max}\Delta t \gg 1$, but were restricted to use at long wavelengths ($kv\,\Delta t \ll 1$) and moderate field gradients (to keep the linearized field prediction valid). This invention is a most useful improvement, allowing efficient integrations on the slow massive ion time scales, essentially attenuating the fast light electron oscillations or other fluctuations at high frequencies.

A fifth step (or several steps) was to integrate the full (or nearly full) Maxwell equation set, driven by J as well as ρ, so as to include the full electromagnetic wave spectrum. An early model using sheets in 1-D3v was by Langdon and Dawson [54] in which the transverse fields were obtained directly from the transverse current and longitudinal field E_x from $-\nabla\phi$ and ϕ from Poisson's equation (as in electrostatic models) (see [12, chaps. 6, 7]). The initial full EM 2-D and 3-D models were by Buneman [22], Boris [18], Morse and Nelson [65], and Langdon and Lasinski [56]. The details of these and later models are in [12, chap. 15] and [2], [56]. Electromagnetic programs are obviously more complicated than electrostatic programs and are generally tougher to use and more expensive computationally.

Suffice it to say that charged-particle ES, MS, and EM simulations have been developed professionally in 2-D and 3-D for a wide variety of applications, such as in fusion (magnetically and inertially confined) and space plasmas. Applications of PIC (CIC) to materially bounded laboratory (low temperature) plasmas are relatively new.

IV. Finite-Size Particle Simulation Theory

A theory of simulation which shows the effects of the numerics, that is, of the finite spatial and temporal steps Δx and Δt, is desirable, along with verification that the simulation theory works. That the validated simulation is truly physics requires checks with both theory and experiment. This section is a brief glimpse of a large amount of material in the three simulation texts mentioned earlier [50], [12], [82].

In the 1960's the simulators using a spatial mesh readily recognized that their simulation plasmas consisted of tenuous *finite-size particles* of a diameter on the order of the size of the mesh (Δx by Δy by Δz).

In the summer of 1968 Okuda and I asked: What are the Coulomb binary collision cross sections for such particles, relative to point particles, but ignoring the computational grid? Our results [68] showed that Coulomb cross sections for clouds are much reduced relative to those for point particles as the cloud radius R is made comparable to λ_D, even for a small number of particles per Debye sphere ($N_D \gtrsim 10$). (Later work in 2-D was given by Matsuda and Okuda [61].) This information was very important for many hot fusion plasma simulations (such as for many waves and instabilities) for which the hot plasma was to be considered essentially collisionless (i.e., $\nu_{\text{collision}}/\omega_p \ll 1$ was desirable). The results also indicated that the Coulomb scattering was mostly at small angles (as in warm laboratory plasmas) involving large impact parameters well approximated by the impulse approximation, even for $N_D \sim 2$; and it follows that the velocity dependence of σ_{clouds} is the same as that for σ_{points}. This information also confirmed our ability to simulate plasmas accurately using clouds with vastly fewer particles per significant volume (λ_D or λ_D^2 or λ_D^3 in 1–3-D) than in the laboratory. (Dawson [33] had already shown that much of the kinetic behavior of a plasma in 1-D could be obtained from a sheet model with $N_D = n\lambda_D \sim 10$.)

At about the same time, Langdon began (in Berkeley) a comprehensive theory of plasma simulation, stimulated by Okuda's calculations and simulations and by earlier discussions with Dawson (at Princeton). The initiation of the theory of simulation thus had at least four players (Dawson, Langdon, Okuda, and myself). We also had the benefit of prior collaborations with my students J. A. Byers and A. Hasegawa in Berkeley and T. Kamimura in Japan—certainly on weightings and finite-size particle notions.

Let us look briefly at the theoretical modeling and some results. The theory shows, for example, that a choice of a too small Debye length ($\lambda_D/\Delta x \lesssim 0.3$) leads to a numerical instability, even with a Maxwellian velocity distribution. Now, in RF discharges, ion charge exchange produces ions at gas (room) temperature, with very small λ_{Di}, so that $\lambda_{Di}/\Delta x \lesssim 0.3$ is readily possible. This instability may be part of the strange heating which has been observed.

The beginnings are as follows (from Langdon and Birdsall [55], as found in [12, p. 65]:

The use of a spatial grid, with interpolation to obtain the charge density, leads to the appearance of charges that are at least one cell wide. This appearance comes from *making observations at the grid points* and from the fact that the fields are calculated from these observations. The corollary is that the particles never behave as if they had zero thickness. Hence, it is wise to be concerned with the *effective shape* of the particles, through the *particle shape factor* $S(\boldsymbol{x})$ and the Fourier transform of the shape factor $S(\boldsymbol{k})$.

The particles have a spread-out charge distribution and move rigidly without rotation or internal change and pass freely through one another. It seems natural to call these particles *clouds*. The interactions of the system of clouds is a straightforward generalization of the point particle interaction; in fact, certain divergences in the kinetic theory and in classical electromagnetic theory are removed.

The charge density at laboratory coordinate $\boldsymbol{x}'$ of a cloud whose center is at $\boldsymbol{x}$ is changed from $q\delta(\boldsymbol{x}' - \boldsymbol{x})$ for a point particle, to $qS(\boldsymbol{x}' - \boldsymbol{x})$ for a cloud, where q is the total charge given by $q\int d\boldsymbol{x}' S(\boldsymbol{x}' - \boldsymbol{x})$. Let $\boldsymbol{J}_p$ and ρ_p be the current and charge densities of a system of point charges located at the $(\boldsymbol{x}')$'s; then the densities $\boldsymbol{J}_c$ and ρ_c for a system of clouds, whose centers coincide with the point particles, are:

$$\begin{bmatrix} \rho_c(\boldsymbol{x},t) \\ \boldsymbol{J}_c(\boldsymbol{x},t) \end{bmatrix} = \int d\boldsymbol{x}'\, S(\boldsymbol{x}' - \boldsymbol{x}) \begin{bmatrix} \rho_p(\boldsymbol{x}',t) \\ \boldsymbol{J}_p(\boldsymbol{x}',t) \end{bmatrix}. \tag{13}$$

These cloud densities are to be used in Maxwell's equations to find the fields $\boldsymbol{E}$ and $\boldsymbol{B}$. The Newton–Lorentz force on one cloud of total charge q, with (center) position $\boldsymbol{x}$ and velocity $\boldsymbol{v}$, is then:

$$\boldsymbol{F}(\boldsymbol{x},\boldsymbol{v},t) = q\int d\boldsymbol{x}'\, S(\boldsymbol{x}' - \boldsymbol{x}) \cdot [\boldsymbol{E}(\boldsymbol{x}',t) + \boldsymbol{v} \times \boldsymbol{B}(\boldsymbol{x}',t)]. \tag{14}$$

These relations are convolutions and, therefore, take on a very simple form when Fourier transformed in space:

$$\begin{bmatrix} \rho_c(\boldsymbol{k},t) \\ \boldsymbol{J}_c(\boldsymbol{k},t) \end{bmatrix} = S(\boldsymbol{k}) \begin{bmatrix} \rho_p(\boldsymbol{k},t) \\ \boldsymbol{J}_p(\boldsymbol{k},t) \end{bmatrix} \tag{15}$$

$$\boldsymbol{F}(\boldsymbol{k},\boldsymbol{v},t) = qS(-\boldsymbol{k})[\boldsymbol{E}(\boldsymbol{k},t) + \boldsymbol{v} \times \boldsymbol{B}(\boldsymbol{k},t)] \tag{16}$$

where

$$S(\boldsymbol{k}) = \int d\boldsymbol{x}\, S(\boldsymbol{x})\, \exp(-i\boldsymbol{k} \cdot \boldsymbol{x}). \tag{17}$$

Our transform convention is such that in the point particle limit (*particle radius* $R \to 0$) or long-wavelength limit $k \to 0$, $S(\boldsymbol{k}) \to 1$. The size of the cloud by some criterion is denoted by R; then $S(\boldsymbol{k})$ becomes small for $|\boldsymbol{k}| \geq R^{-1}$.

The shape factor S need not be isotropic (and has not been in practice, e.g., squares and cubes) or symmetric (but usually is). However, in this section we assume that $S(\boldsymbol{x})$ is isotropic. Therefore $S(\boldsymbol{k})$ is isotropic and real valued. (For asymmetrical clouds, the only change in most results is to replace $S^2(\boldsymbol{k})$ with $|S^2(\boldsymbol{k})|$.)

Using (15) and a little care, one can now redo most plasma theory with few changes by the replacement of the charge q by $qS(\boldsymbol{k})$. For example, the dielectric tensor for a uniform Vlasov gas of clouds and therefore, dispersion relations, are unchanged except that the plasma frequency squared ω_p^2 must everywhere be multiplied by $S^2(\boldsymbol{k})$ (one S from the equation of motion, another from relating position to density) as:

$$\omega^2 \approx S^2(\boldsymbol{k})\omega_p^2. \tag{18}$$

This result may be viewed as a k-dependent plasma frequency or charge when adapting linear stability analyses, etc., to cloud plasmas.

We look at longitudinal plasma oscillations to see how the simulation differs from the physics for point particles.

The longitudinal dielectric function for a cloud plasma for small perturbations is:

$$\varepsilon(k,\omega) = 1 + S^2(k)\frac{\omega_p^2}{k^2}\int \boldsymbol{k} \cdot \frac{\partial f_0}{\partial \boldsymbol{v}} \frac{d\boldsymbol{v}}{\omega - \boldsymbol{k} \cdot \boldsymbol{v}} \tag{19}$$

with the standard symbol definitions. Space-time dependence $\exp(i\boldsymbol{k} \cdot \boldsymbol{x} - i\omega t)$ is assumed and the usual remarks about analyticity apply. For a Maxwellian velocity distribution with no drift and thermal velocity, $v_t = [v_{av}^2/3]^{1/2}$, the dielectric function becomes:

$$\varepsilon(k,\omega) = 1 - \frac{1}{2}\left(\frac{S\,\omega_p}{kv_t}\right)^2 Z'\left(\frac{\omega}{\sqrt{2}}\, kv_t\right) \tag{20}$$

where Z' is the derivative of the plasma dispersion function of Fried and Conte [41].

We now add the spatial grid where the force on a particle depends not only on the distance to neighboring charges, but also on the particle position relative to the grid. Birdsall and Langdon [12, p. 162] say:

The *grid charge density* ρ_j is obtained from the charges q_i located at positions x_i from:

$$\rho_j \equiv \rho(X_j) = \sum_i q_i S(X_j - x_i). \tag{21}$$

This can be interpreted as the charge density for *finite-size particles,* sampled on the grid through zero-, first-, or second-order interpolation (higher order is seldom used).

For ρ_j, an *electric field is found on the grid,* usually the same grid. In electrostatic problems this is usually done by solving finite-difference forms of $\nabla^2\phi = -\rho$ and $\boldsymbol{E} = -\nabla\phi$; there is nothing in the present analysis to require use of any particular form or smoothing or emphasis.

The *force on the particle* is interpolated from the grid electric field as:

$$F_i = q_i\, \Delta x \sum_j E_j S(X_j - x_i) \tag{22}$$

using the *same* weighting function S as in (21). Although using the same weight functions in (21) and (22) are not a necessary feature of this discussion, there are good reasons for doing so. Using different weight functions in (21) and (22) corresponds to using different cloud shapes, which can lead to a gravitation-like instability. Also, if the difference equations relating ρ_j and E_j are symmetric in space, *use of the same weight function eliminates the self-force* and ensures conservation of momentum. Various interpolating functions, with which we already are familiar as shape factors, are shown in the figure (Fig. 7).

Let us look at the force field $F(x)$ for *linear interpolation* as shown in the figure (Fig. 8). It varies as a set of straight line segments; the segments give rise to *spatial harmonics* of

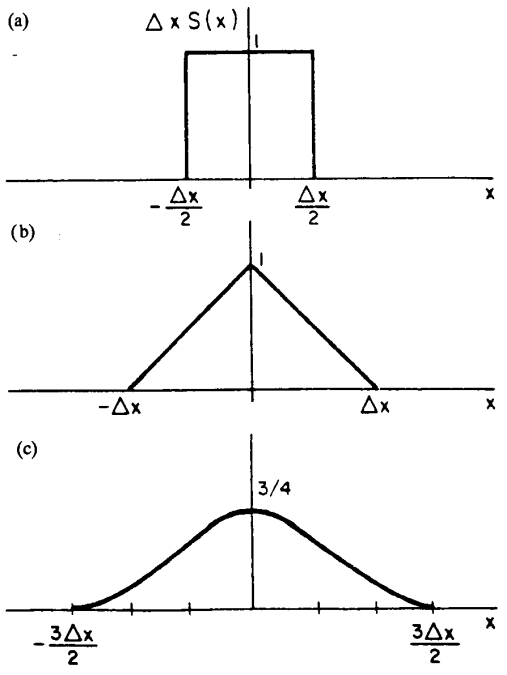

Fig. 7. Various interpolating functions for charge and force: (a) Zero-order (NGP); (b) first-order (CIC, PIC); and (c) second-order (parabolic or quadratic) spline, consisting of three parabolic sections of length Δx, joined with no discontinuities in the slope. (From Birdsall and Langdon [12].)

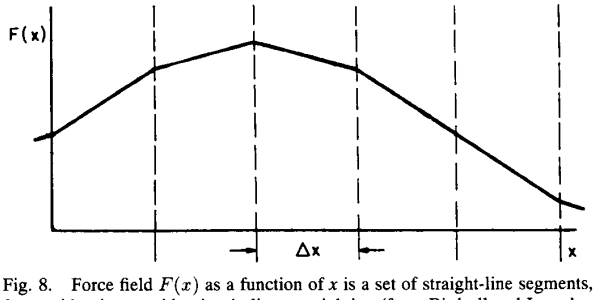

Fig. 8. Force field $F(x)$ as a function of x is a set of straight-line segments, from grid point to grid point, in linear weighting (from Birdsall and Langdon [12]).

period $\sim \Delta x$; stated another way, the particles "feel" the grid.

We can now deal in detail with the effects of the spatial grid, as done by Langdon and Birdsall [55], and found in [12, p. 158 *ff.*]:

Let us consider the interaction force $F(x_1, x_2)$, defined as the force on a particle at x_2 due to a particle at x_1 in one dimension. In a normal physical system, which is invariant under displacement, F depends only on the separation $x \equiv x_2 - x_1$. However, in a computer simulation using a spatial grid, invariance does not exist under all displacements (displacing particles but not the grid). Thus *F also depends on the location relative to the grid, $\overline{x} \equiv \frac{1}{2}(x_1 + x_2)$ as well as x* (Fig. 9). *In most simulations a grid with constant spacing Δx is used; in*

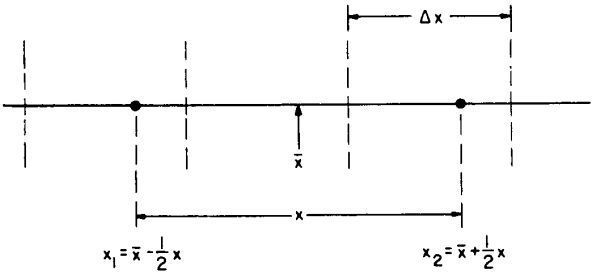

Fig. 9. Notation in one dimension. Two particles are located at x_1 and x_2, with separation $x = x_2 - x_1$ and mean position $\overline{x} = (x_2 + x_1)/2$. A grid of spacing Δx is imposed on the space (from Birdsall and Langdon [12]).

this case the force $F(\overline{x} - \frac{1}{2}x, \overline{x} + \frac{1}{2}x)$, considered as a function of displacement $\overline{x}$ with separation constant, is periodic with period Δx.

In order to study the effect of the nonuniformity on a plasma, we need the Fourier transform of $F(x_1, x_2)$. For an *infinite system* we use a Fourier integral transform in x and a Fourier series in $\overline{x}$:

$$F\left(\overline{x} - \frac{1}{2}x, \overline{x} + \frac{1}{2}x\right) = \int_{-\infty}^{\infty} \frac{dk}{2\pi} e^{ikx} \sum_{p=-\infty}^{\infty} e^{ipk_g\overline{x}} F_p(k) \tag{23}$$

where

$$k_g \equiv \frac{2\pi}{\Delta x}$$

is the *grid wave number,* and

$$F_p(k) = \int_{-\infty}^{\infty} dx\ F_p(x) e^{-ikx} \tag{24}$$

$$F_p(x) = \frac{1}{\Delta x} \int_{\Delta x} d\overline{x}\, e^{-ipk_g\overline{x}} F\left(\overline{x} - \frac{1}{2}x, \overline{x} + \frac{1}{2}x\right). \tag{25}$$

This sign and normalization for the Fourier integral are followed throughout.

Those properties of the plasma which are little affected by the lack of displacement invariance are expected to be similar to those of a plasma with two-particle force equal to the $p = 0$ or *average force* $F_0(x)$; such properties can be analyzed by the gridless theory (Langdon and Birdsall [55]). The difference $\delta F = F - F_0$ is a *nonphysical grid force.* In some respects, δF is like a "noise" force; however, it is coherent with the plasma perturbation.

Let the particle density be $n(x, t)$ (actually n is a sum of δ functions when the number of particles in finite). Then the force $F(x)$ on a particle at x is (time dependence ignored for now):

$$F(x) = \int dx'\, F(x', x) n(x'). \tag{26}$$

When transformed, this becomes, using (23):

$$F(k) = \sum_{-\infty}^{\infty} F_p\left(k - \frac{1}{2}pk_g\right) n(k_p) \tag{27}$$

where

$$k_p \equiv k - pk_g. \tag{28}$$

We see that the effect of δF (corresponding to the $p \neq 0$ terms) is to *couple density perturbations and forces at wave numbers*

which differ by integral multiples of the grid wave number k_g. Such wave numbers are said to be *aliases* of one another.

With this foundation, plus some work with finite differences for the gradient $\boldsymbol{k} \to \boldsymbol{\kappa}(k_p)$ Laplacian $k^2 \to K^2(k)$, one obtains (copied from [12, p. 177]):

The dielectric function for an unmagnetized electrostatic Vlasov plasma is:

$$\varepsilon(\boldsymbol{k},\omega) = 1 + \frac{\omega_p^2}{K^2(\boldsymbol{k})} \sum_p |S(\boldsymbol{k}_p)|^2 \int \frac{d\boldsymbol{v}}{\omega + i0 - \boldsymbol{k}_p \cdot \boldsymbol{v}} \boldsymbol{\kappa} \cdot \frac{\partial f_0}{\partial \boldsymbol{v}}, \quad \text{Im } \omega \geq 0. \tag{29}$$

For f_0, a Maxwellian velocity distribution with no drift, (29) becomes:

$$\varepsilon(\boldsymbol{k},\omega) = 1 - \frac{\omega_p^2}{2K^2 v_t^2} \sum_p |S(\boldsymbol{k}_p)|^2 \frac{\boldsymbol{\kappa} \cdot \boldsymbol{k}_p}{k_p^2} Z'\left(\frac{\omega}{\sqrt{2}\,|\boldsymbol{k}_p| v_t}\right) \tag{30}$$

where Z' is the derivative of the plasma dispersion function (Fried and Conte, 1961).

When $\lambda_D \geq \Delta x$ the principal term is the one whose $\boldsymbol{k}_p$ is nearest $\boldsymbol{k}$. The modes are heavily damped when $\boldsymbol{k}$ differs much from this $\boldsymbol{k}_p$. In this case we expect no important interaction among the different aliases. In the first zone let us take *only* the $\boldsymbol{p} = 0$ term, obtaining the average force $\boldsymbol{F}_0$ dielectric function ε_0 discussed earlier. We then view the model as approximately a gridless cloud plasma with Coulomb interaction having:

$$\varepsilon_0 = 1 - \frac{\omega_p^2}{2k^2 v_t^2} |S_0|^2 Z'\left(\frac{\omega}{\sqrt{2} k v_t}\right) \tag{31}$$

with

$$|S_0(\boldsymbol{k})|^2 = |S(\boldsymbol{k})|^2 \frac{\boldsymbol{k} \cdot \boldsymbol{\kappa}}{K^2}, \qquad \text{i.e., } \boldsymbol{p} = 0 \text{ only} \tag{32}$$

where S_0 is the cloud shape factor to be used in the dispersion relation.

Solution of these two dispersion relations (30) and (31) are given in (Fig. 10) for $\lambda_D = \Delta x$ for the Maxwellian in one dimension with $S(k) = \text{dif}\left(\frac{1}{2} k \Delta x\right)$ for NGP. The difference between Im ω in the two cases is too small to be shown on the graph, and Re ω differs significantly only where the wave is heavily damped. Thus alias coupling is not very important for $\lambda_D/\Delta x = 1$ and the averaged force works very well. This conclusion is stronger for CIC–PIC.

There are now many wave phase velocities ω/k_p with which particles may resonantly interact. Unless the coupling is very strong there is no qualitative change in Re ε for real ω; in particular, the sign of its derivative is unchanged. This need not be true for the sign of the imaginary part:

$$\text{Im } \varepsilon = -\pi \frac{\omega_p^2}{K^2} \sum_p \kappa S^2(k_p) \frac{1}{|k_p|} f_0'\left(\frac{\omega}{k_p}\right) \tag{33}$$

so that the plasma stability may be changed. For half the aliases, $\boldsymbol{k}_p$ has the opposite direction to κ so that the factor $\kappa \cdot \boldsymbol{k}_p / k_p^2$ has the wrong sign. For small $k/\Delta x$, this can make ω negative, while $\omega \partial$ Re $\varepsilon/\partial\omega$ remains positive; this leads to an *instability* (Lindman [59]; Langdon [51], [52]). In the jargon of real plasmas, the wave has positive energy and experiences negative absorption. With $\lambda_D = \Delta x$, Langdon (1970) found weak growth occurring only at wavelengths much *greater* than Δx (a surprise). Growth became significant when $\lambda_D/\Delta x$ was decreased, with appreciable growth over a wide range of $k\,\Delta x$, as in (Fig. 11) for $\lambda_D = \Delta x/10$. We now explain these results and come to additional conclusions.

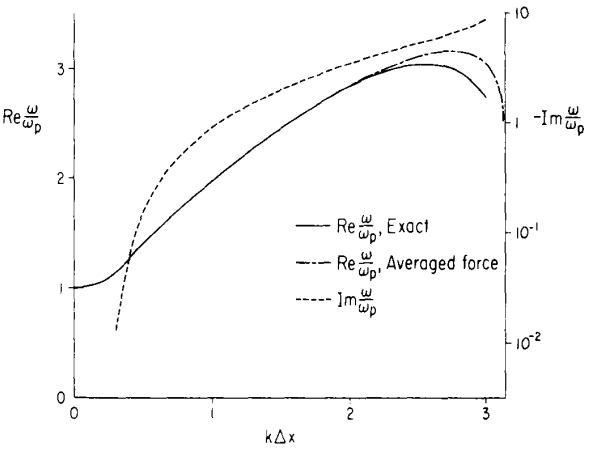

Fig. 10. Solutions of the exact (all p) and average-force ($p = 0$) dispersion relations for a Maxwellian velocity distribution with $\lambda_D/\Delta x = 1$, NGP interpolation. The *Im* ω is the expected Landau damping (from Langdon [52]).

The dispersion relation is periodic in k; we keep $k < k_g/2, k\Delta x < \pi$ (i.e., in the fundamental Brillouin zone), which is the k one would think of physically. Then the physical phase velocity ω/k is larger than the alias velocities $\omega/k_p, p \neq 0$. Thus ω/k may be much larger than v_t, leading to negligible Landau damping, at the same time that the slow waves are interacting strongly with the thermal particles, as shown in (Fig. 12), if $k_g v_t \gtrsim \omega_p$. The contributions from waves with equal $|p|$ nearly cancel; the net effect turns out to be destabilizing. Although it is small for small $k\Delta x$ (being $\propto (k\Delta x)^2$ for NGP and $(k\Delta x)^4$ for linear weighting), the Landau damping of the principal wave goes to zero even faster as $k \to 0$. Thus the grid can destabilize oscillations even with long wave lengths $\lambda \gg \Delta x$.

For $\lambda_D \geq \Delta x/2$, the alias wave velocities fall on the flat part of the particle velocity distribution and Landau damping occurs unless $k\,\Delta x \leq 2k\lambda_D$ is small. Therefore the instability is confined to long wavelengths and is very weak. A rough rule of thumb is that this nonphysical instability has ignorable growth for $\lambda_D/\Delta x \geq 1/\pi \approx 0.3$ for linear weighting.

However, when $\lambda_D \sim 0.1\Delta x$, the lowest and strongest aliases interact with the steep sides of f_0 and there is little Landau damping, even for $k\,\Delta x \sim 2$ where the coupling is strong. The result is strong instability; Im ω is as large as $0.1\omega_p$ for NGP; however, Im $\omega < 0.014\omega_p$ for linear weighting, which is about 1 dB per plasma cycle, negligible in many applications.

If $\lambda_D/\Delta x$ is decreased further, only the weaker large p aliases contribute and the instability goes away, as it should, since, of course, a cold stationary plasma is inactive (oscillatory only—stable). In many applications, a cold plasma component provides accurate, noise-free collective behavior.

Next, Langdon considered the effects of the finite time step

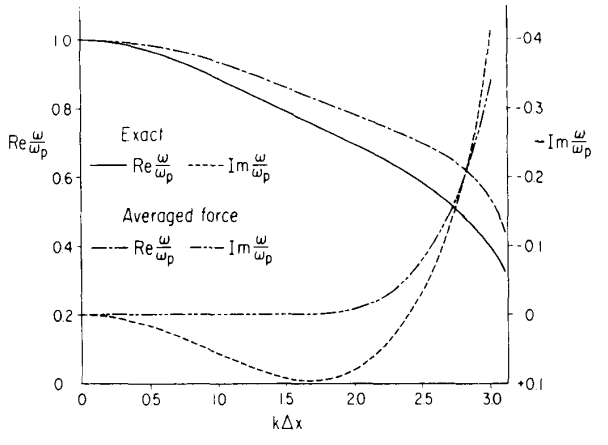

Fig. 11. Solutions of the exact and average-force dispersion relations with $\lambda_D/\Delta x = 0.1$, NGP interpolation. The Im $\omega > 0$ for $0 < k\,\Delta x \leq 2.5$ is nonphysical growth, due to aliasing, arising only if $|p| > 0$ terms are kept. In CIC–PIC, the maximum growth rate is about $0.014\omega_p$, about 10 times smaller (from Langdon [52]).

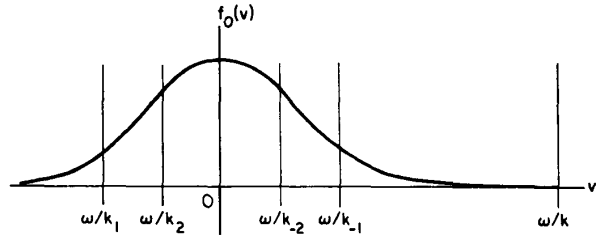

Fig. 12. Wave-phase velocity ω/k and alias wave-phase velocities ω/k_p and $f_0(\nu)$ for $k_g\, v_t \approx \omega_p$ (from Langdon [52]).

on waves, using the leap-frog mover, for an electrostatic model, with no spatial grid (again, from [12, p. 187]):

The dispersion function ε is

$$\varepsilon(\boldsymbol{k},\omega) \equiv 1 - \omega_p^2 \int \frac{d\boldsymbol{v} f_0(\boldsymbol{v})}{\left[(2/\Delta t)\sin\tfrac{1}{2}(\omega + i0 - \boldsymbol{k}\cdot\boldsymbol{v})\,\Delta t\right]^2} \tag{34}$$

$$= +\frac{\omega_p^2}{k^2}\int d\boldsymbol{v}\,\boldsymbol{k}\cdot\frac{\partial f_0}{\partial v}\,\frac{\Delta t}{2}\,\cot(\omega + i0 - \boldsymbol{k}\cdot\boldsymbol{v})\frac{\Delta t}{2} \tag{35}$$

and ω_p is the plasma frequency. The second form is obtained by an integration by parts; in the limit $\Delta t \to 0$, it reduces to the familiar plasma result. The dispersion function ε plays the usual role in other results, such as for shielding and fluctuations. In a multispecies plasma, each species contributes.

The term "$i0$" in (34) and (35) reminds us that it was derived assuming Im $\omega > 0$, but may be used for real ω or even damped oscillations by analytic continuation to or below the real ω axis, just as in the usual Landau damping analysis.

V. Early Work on Simulation Electron-Neutral Elastic Collisions

Burger [28] showed a method of doing electron-neutral elastic collision for his simulations with low-pressure diodes. His method, while used for only one kind of collision, is very similar to the PIC–MCC we will present later on which allows for many kinds of collisions. Hence his work is the earliest PIC–MCC we have found. Here is his description (with some parts omitted):

In order to account for randomizing collisions, the velocity of each charge carrier has to be given in at least two directions—or what is equivalent, we have to know the total energy of the particle in addition to its velocity component in the x direction. The particle is still advanced according to the x velocity component only. The total energy of a particle influences the probability that the charge carrier will suffer a collision in a time interval Δt. Also, the total energy of the particle is the quantity which is conserved in an elastic collision.

In our computer calculations we store an additional quantity to those described earlier $[x(t_n), v_x(t_{n-1})]$: the quantity $v_\perp^2(t_n)$, the square of the component of the particle's velocity lying in the plane perpendicular to the x direction. We set $v_x(t_n) = [x(t_n) - x(t_{n-1})]/\Delta t$ and assume that the charge carrier travels at this velocity during the time interval $t_{n-1} \leq t \leq t_n$. To calculate the effect of collisions we need only the magnitude of the total velocity of the particle, which is:

$$v(t_n) = \left[v_x^2(t_n) + v_\perp^2(t_n)\right]^{1/2}. \tag{36}$$

We should expect that the error in the assumption that the particle travels with velocity $v(t_n)$ during the interval $t_{n-1} \leq t \leq t_n$ will decrease as we decrease Δt.

If we know the mean-free path as the function of electron energy, i.e., total velocity for the particular collision process we want to study, than we can calculate the probability of a collision for a given particle that travels with velocity $v(t_n)$ for a time interval Δt by the following expression:

$$P_c(t_n) = 1 - \exp\{-v(t_n)\,\Delta t/\lambda[v(t_n)]\} \tag{37}$$

where P_c is the probability that this particle suffers a collision during the time interval $t_{n-1} \leq t \leq t_n$, and $\lambda(v)$ is the mean-free path given as the function of velocity. The probability given by (37) is evaluated for all the particles at every time step from the quantities $v^2(t_n)$, $v_x(t_n)$. After this calculation is made the decision has to be reached as to which particles should suffer collisions. Obviously, this decision should be made in a random manner. In the following examples only hardsphere collisions were considered with constant mean-free path, so λ was a constant. But (37) is valid for any known function of $\lambda(v)$ and therefore the calculations could be made for any known law of scattering process. Since the velocity of the particle is recalculated at each time step, the effect of a variable cross section is incorporated in the calculations and the error will be small if the change in the velocity of the particles is small between time steps. This requires a small time step again.

The decision as to which particle should suffer a collision was made in the following manner. The diode space was divided into 128 equal regions in the x direction. In each region the probabilities P_c were calculated for the particles, and using the sequence in which they were recorded, their probabilities were added. The particle whose probability made this sum larger than one suffered a collision, and the summing of probabilities was restarted with the sum decreased by one. The sums were saved from step to step, and summing was always resumed where it was left off one time-step earlier. The described procedure insures that on the average, the number

of particles that make collisions in a small region of the diode is equal to the expectation value calculated from their probabilities. Since particles travel from region to region fairly rapidly and are injected in a random manner, their sequence in storage could also be considered random.

Once we have decided that a particle will suffer a collision, we have the problem of determining the two components of its velocity after the collision has taken place v_x^*, $(v_\perp^*)^2$ (where the star indicates quantities after the collision). The first assumption we make is that there is no energy loss due to the collision. This assumption means that the neutrals have infinite mass and zero velocity in the laboratory frame. Consequently, the equation

$$(v_x^*)^2 + (v_\perp^*)^2 = v_x^2 + v_\perp^2 \tag{38}$$

must hold, and we can choose only one velocity component freely. The selection of this velocity component (we selected v_x^* in our calculations) depends upon the angle dependence of the collision process under study, and, in general, it is a function of v_x and $v_\perp$. We again simplified our calculations by assuming hard-sphere collisions. This process has no preferred direction; therefore the distribution of velocities v_x^* is uniform in the interval $-v \le v_x^* \le v$. We have generated a sequence of random numbers in the computer whose distribution was uniform in the unit interval and used the number from this sequence (R) to determine the x component of the velocities of particles that suffered collisions. The equation $v_x^* = \pm Rv$ was used, with the sign alternating from collision to collision.

After v_x^* has been chosen for the colliding particle, (38) is used to determine $(v_\perp^*)^2$, which is then stored and used for this particle at successive time steps until the next collision takes place.

This is a simple method of including electron-neutral collisions.

VI. Early Work on Simulating Electron–Ion Coulomb Collisions, Lorentz Gas Model

Shanny *et al.* [76] showed their method for adding electron collisions with massive ions, the so-called Lorentz gas model. (The self-consistent part of the model is that of Dawson, with electron sheets moving in a uniform fixed ion background.) We paraphrase their work as follows (from Berkeley course notes on their article):

The electrons scatter in $3v$ through small-angle collisions with the stationary ions. There is no exchange of energy between e and i; the only energy exchange is between the longitudinal motion (velocity v_z, along z, the 1-D) and the transverse motion (velocity $v_\perp > 0$, along x and y) due to scattering by the ions.

Collisions between sheets and background ions are taken into account as follows. During Δt, a number of small angle collisions may have taken place, each with a different orbit plane. The result is to change the direction of the velocity, but not its magnitude; the velocity vector stays on a spherical surface in v space, with deflection described by two angles ϕ and ψ, as shown in (Fig. 13). α is the initial inclination of the velocity vector to the z axis; ϕ is the magnitude of the angle of deflection; and ψ is the orientation of the scattering around the deflection cone. Angle ψ is chosen randomly, with a uniform distribution $2\pi R_1$, $0 < R_1 < 1$ and uniform. The distribution of ϕ is chosen so as to agree with the Spitzer (1962)

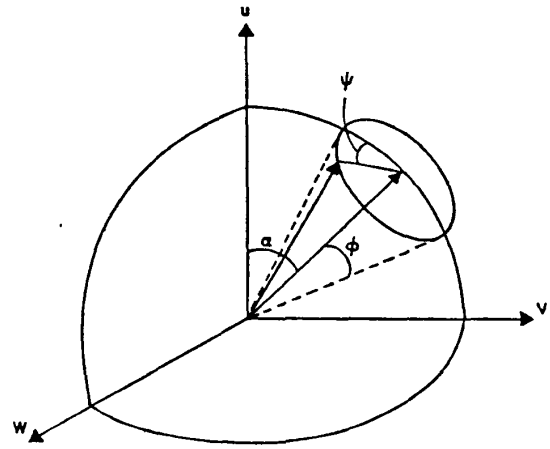

Fig. 13. Scattering of the velocity vector. The quantity α is the initial inclination of the velocity vector to the x axis, ϕ is the magnitude of the scattering, and ψ is the orientation of the scattering relative to the x axis (from Shanney *et al.* [76]).

formula for small-angle scattering; the differential probability for a scattering lying in the range ϕ to $\phi + d\phi$ to occur in a time Δt is:

$$P(\phi)\,d\phi = \left(\phi\,d\phi/\langle\phi^2\rangle\,\Delta t\right)\exp\left[-\phi^2/2\langle\phi^2\rangle\,\Delta t\right] \tag{39}$$

where

$$\langle\phi^2\rangle = \frac{3\omega_p}{2}\frac{\ln\Lambda}{\Lambda} \tag{40}$$

and

$$\Lambda = \frac{6\pi n}{Z}\left[\left(v_z^2 + v_\perp^2\right)/\omega_p^2\right]^{3/2} \tag{41}$$

with Z/n a constant that can be chosen for convenience. (The $[\ ]^{3/2}$ is taken as λ_D^3, so that their

$$\Lambda = \frac{6\pi n}{Z}\lambda_D^3 = \frac{6}{Z}\left(\frac{4}{3}\pi n\,\lambda_D^3\right)\frac{3}{4} = \frac{9N_D}{2Z}. \tag{42}$$

This seems to leave Z to be chosen for convenience, if the N_D of Λ in the expression are the simulation values (which is *not* necessary).) We need to invert the cumulative distribution function:

$$C(\phi) = \int_0^\phi P(\phi)\,d\phi \tag{43}$$

meaning that ϕ is the inverse of C, to be set equal to a uniform set of numbers R_2, $0 < R_2 < 1$,

$$\phi = C^{-1}(R_2). \tag{44}$$

Fortunately, $P(\phi)\,d\phi$ can be integrated to produce:

$$R_2 = C(\phi) = 1 - \exp\left[-\phi^2/\left(2\langle\phi^2\rangle\,\Delta t\right)\right] \tag{45}$$

and then inverted to produce the desired scattering angle,

$$\phi(R_2) = \left[-2\langle\phi^2\rangle\,\Delta t\,\ln(1 - R_2)\right]^{1/2}. \tag{46}$$

Shanny *et al.* showed that this collision term, cumulated over many increments in time and in the limit that Δt becomes small, simulates a Lorentz gas collision term of the form:

$$\frac{\partial}{\partial t}P(V,\theta,t) = \nu(V)\frac{1}{\sin\theta}\frac{\partial}{\partial\theta}\sin\theta\frac{\partial}{\partial\theta}P(V,\theta,t) \tag{47}$$

where $u = V\cos\theta$, $v = V\sin\theta$. The collision frequency ν is:

$$\nu = \frac{1}{2}\langle\phi^2\rangle \tag{48}$$

and is velocity dependent, behaving like $1/v^3$, as noted from (41) (ignoring the v dependence of ln Λ), as is desired physically.

The application is straightforward. At t, the velocity vector of a particle has an angle α away from what is declared the z or v_z axis toward the $v_\perp$ axis. The new particle velocity vector will have the same magnitude, but moved away from α by the deflection cone angle ϕ obtained from (46) using R_2 and with $\langle\phi^2\rangle$ calculated from (40) for that particle (ensuring the proper velocity dependence) and at angle ψ selected by R_1.

Let us be even more specific by putting in the $3v$ spherical coordinate transformations explicitly. (Work done in Berkeley by J. Harte, with thanks.) First, find the angles of the initial velocity vector; this has components v_x, v_y, and v_z, with v_z taken as the polar axis. Define:

$$v_\perp^2 = v_x^2 + v_y^2, \qquad \sin P = v_y/v_\perp, \qquad \cos v_x/v_\perp \tag{49}$$

$$v^2 = v_\perp^2 + v_z^2, \qquad \sin\alpha = v_\perp/v, \qquad \cos\alpha = v_z/v \tag{50}$$

α and T are *not* to be found; they are names of ratios to be used later. Second, put in the collision frequency velocity dependence by calculating $Q(v)$, in place of $2\langle\phi^2\rangle\Delta t$, from:

$$Q(v) \equiv C/v^3 \tag{51}$$

where C is a specified constant, proportional to the magnitude of v (obtainable from (40), (41), (48)). The angle ϕ is now calculated from (46) as:

$$\phi = [-Q\ln(1 - R_2)]^{1/2} \tag{52}$$

and angle ψ is:

$$\psi = R_1(2\pi) \tag{53}$$

where R_1 and R_2 are independent random numbers. Third, look up $\sin\phi$, $\cos\phi$, $\sin\psi$, and $\cos\psi$ and then calculate the velocity increments by components as:

$$\begin{aligned}
\Delta v_x &= v[\sin\phi\sin\psi\cos\alpha\cos P - \sin\phi\cos\psi\sin P \\
&\quad - 2\sin^2\frac{\phi}{2}\sin\alpha\cos P] \\
\Delta v_y &= v[\sin\phi\sin\psi\cos\alpha\sin P - \sin\phi\cos\psi\cos P \\
&\quad - 2\sin^2\frac{\phi}{2}\sin\alpha\sin P] \\
\Delta v_z &= v[-\sin\phi\sin\psi\sin\alpha - 2\sin^2\frac{\phi}{2}\cos\alpha].
\end{aligned} \tag{54}$$

Lastly, add these increments to the initial components:

$$\begin{aligned}
v_{x\text{new}} &= v_x + \Delta v_x \\
v_{y\text{new}} &= v_y + \Delta v_y \\
v_{z\text{new}} &= v_z + \Delta v_z.
\end{aligned} \tag{55}$$

Obviously, one may make simplifications; e.g., use R_2' in place of $1 - R_2$; calculate combinations once, such as $\sin\phi\ \sin\psi$; use $\sin\frac{\phi}{2}$ and $\cos\frac{\phi}{2}$ in (54) more efficiently than $\sin\phi$ and $\sin^2\frac{\phi}{2}$; consider replacing $\sin\phi$ by ϕ and $\cos\phi$ by 1; etc. As the process is repeated for each particle each time step, any and all simplifications should be considered.

Collisional processes other than the Lorentz gas may also be calculated, given the scattering probabilities and obtaining the inverse cumulative distributions (analytically or numerically).

Again, like Burger [28], elements of MCC are present here.

VII. Early PIC–MCC Work for Including Coulomb Collisions

As noted earlier, in the particle-mesh approach, short-range particle–particle interactions are smoothed, if not lost. Hence to recover the velocity scatterings associated with interparticle spacings or impact parameters less than a mesh cell diameter Δx, it is necessary to add particle–particle interactions to the particle-mesh scheme.

A hybrid called PPPM or P^{3}M in [50, chap. 8] splits the interparticle force into a short range part $\boldsymbol{f}^{\text{sr}}$ (inside a radius r_e) and a smoothly varying part $\boldsymbol{R}$ (with $R(k)$ band limited); hence long-range and Coulombic, using both a coarse chaining mesh (cell diameter $\approx r_e$) and a finer charge/potential mesh (such that $\Delta x < \lambda_D$). Then the pairs of particles to be located and used for f^{sr} must be identified economically, hopefully without sweeping through all of the possible pairs. Hockney and Eastwood [50, secs. 8-4-1–3) show how to do this with savings of two orders of magnitude in computer time. More details are in [38].

A binary collision model was made for Coulomb collisions, employing Monte Carlo techniques, in 1-D3v by Takizuka and Abe [81] and further development by Procassini *et al.* [71]. Charged particles within a given spatial grid cell are scattered off each other, pair-wise ($e - e$, $e - i$, and $i - i$), by going to the target-particle-at-rest frame, binary scattering, and then back, explicitly conserving momentum and implicitly conserving energy. The checks indicate good behavior. The process is computationally intensive, with substantial increases in running times, but is chosen when careful energy and momentum exchanges are desired. (See Procassini and Cohen [72] regarding codes TESS and DIPSI.)

VIII. Bounded Plasma Device Codes

For many years plasma simulations were focused on the behavior of the bulk of the plasma, as there are many oscillations, waves, instabilities, and transport problems in the bulk. Gentle density gradients were included, as were plasma–vacuum interfaces; when particles approached a boundary, they usually were specularly or otherwise reflected so as to create no edge physics. For many such models, periodic boundary conditions were acceptable, essentially ignoring boundaries. Indeed, in all plasma studies (theory, experiment, simulation) there is a ratio of about 100 000 to 1000 publications on the bulk plasma to those on the edge plasma, respectively.

Hence adding realistic boundaries to plasma models in analysis and simulation is like sailing in almost uncharted waters. However, in the past decade, edge plasma modeling has advanced considerably from the early works of Langmuir and Tonks and Bohm. There are several strong motivations: One is the desire to describe (and maybe control) plasma edge transport in all kinds of fusion hot plasma devices, focusing mainly on tokamak walls, limiters, and diverters; the plasma temperature drops from fusion values (10's of keV) to wall-tolerable values, sometimes in a few centimeters, with considerable plasma-edge–surface interaction (collisional, cooling, recycling, sputtering, etc.). Another is the desire to model dc, RF, and microwave discharges used in plasma-assisted materials processing (PAMP), such as for etch-

ing, sputtering, deposition, and implantation. Again, modeling knowledge is used to improve control.

We began our plasma-sheath-bounded modeling in Berkeley about 10 years ago, first aimed at fusion plasma edges. (Actually, D. Fuss and I had a 48 by 48 cell 2-D3v bounded code SQRPLA running at LLNL in 1968, with neutral-beam injection, ionization, and modeling magnetic mirror machines.) Stimulated by the growth of PAMP and especially by the analytic models and experiments of my colleague, M. A. Lieberman, and the fluid and particle models of another colleague, D. B. Graves (Chem. Engr.), my plasma theory and simulation group has become heavily involved in modeling and simulating low-pressure plasma discharges in a number of applications. Remarkably, working on both the fusion and processing plasma edges and sheaths has had challenging and productive cross fertilizations.

So how do we simulate bounded plasmas? Some initial work is in [12, chap. 16] on various aspects of handling charges at the boundaries and on coupling to external circuit elements and sources. A more complete report is by Lawson, who wrote our first planar 1-D3v bounded PIC code, PDW1 in 1983; this code is in FORTRAN. Using PDW1 as a base, re-done in C with considerable additions, including MCC, we now have three codes for interactive use on fast PC's and workstations, with numerous applications: 1-D3v for planar or concentric cylinder of concentric spherical electrodes (PDP1, PDC1, PDS1).[1] The analytic and numerical modeling as developed by my students, Verboncoeur *et al.* [89] is given here, much shortened, as follows.

The planar, cylindrical, and spherical configurations for one-dimensional bounded plasma systems are shown in Figs. 14 and 15.

The current in the external circuit interacts with the plasma current via surface charge on the electrodes. Similarly, the potential within the plasma region is affected by the distribution and motion of space charge, the electrode surface charge, and the current in the external circuit. Thus we seek a simultaneous solution for the potential and circuit equations.

The boundary conditions for the potential equation are obtained by applying Gauss's Law to the system:

$$\int_S \boldsymbol{E}\cdot d\boldsymbol{S} = \int_V \frac{\rho}{\varepsilon}\,dV + \frac{A_+\sigma_+ + A_-\sigma_-}{\varepsilon} = 0 \qquad (56)$$

where the surface S encloses the plasma and electrodes. Area A_+ refers to the surface area of the positively biased (left/inner) electrode, A_- to the negatively biased (right/outer) electrode, and σ is the surface-charge density on the respective electrode. Note that ρ has units of charge/volume and σ has units of charge/area. Equation (56) is a statement of Gauss's Law; the first part reflects the assumption of an ideal conductor connecting the electrodes to the external circuit elements, the second part, conservation of charge in the system.

Applying Gauss's Law about each node of the gridded system and using the definition of potential, we obtain the following finite-difference equations:

planar grid

$$\frac{\Phi_{j+1} - 2\Phi_j + \Phi_{j-1}}{\Delta x^2} = -\frac{\rho_j}{\varepsilon} \qquad (57)$$

cylindrical grid

$$r_{j+1/2}\Phi_{j+1} - 2r_j\Phi_j + r_{j-1/2}\Phi_{j-1} = -\frac{r_j\Delta r^2}{\varepsilon}\rho_j \qquad (58)$$

[1]Available from Software Distribution Office, Industrial Liaison Program, EECS Dept., Cory Hall, University of California, Berkeley, CA 94720.

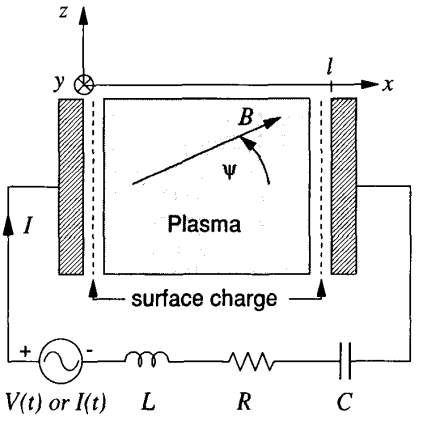

Fig. 14. One-dimensional planar model, displacement of particles along x, but with three velocity components with external circuit sources (from Verboncoeuer *et al.* [89]).

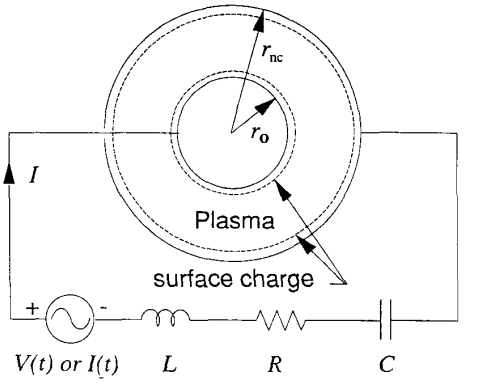

Fig. 15. Configuration in cylindrical and spherical coordinates with series RLC circuit and voltage/current source. Particles are cylindrical shells with displacement in the radial direction in cylindrical coordinates, and spherical shells with radial motion in spherical coordinates, but with all three velocity components (from Alves *et al.* [3]).

spherical grid

$$r_{j+1/2}^2\Phi_{j+1} - \left(r_{j+1/2}^2 + r_{j-1/2}^2\right)\Phi_j + r_{j-1/2}^2\Phi_{j-1} = -\frac{\left(r_{j+1/2}^3 - r_{j-1/2}^3\right)\Delta r}{3\varepsilon}\rho_j . \qquad (59)$$

In the cylindrical and spherical forms, $r_{j+1/2} = r_j \pm \Delta r/2$. (We have also used nonuniform Δr, for example, for spherical probe or particulate problems, with smaller Δr at the probe.) For (57)–(59), $j = 1, 2, \cdots, nc-1$, where nc is the number of cells in the gridded space. These results are equivalent to the flux-conserving method of [12, sec. 14-10]. The planar and cylindrical result of (57) and (58) can also be obtained by applying a central difference to the Poisson equation; the finite difference result is different in spherical coordinates.

For a one-dimensional system, the boundary conditions used are:

$$\Phi_{nc} = 0 \qquad (60)$$

and

$$E_0 = \frac{\sigma_+}{\varepsilon}. \tag{61}$$

Equation (60) fixes a reference potential for the system without implying a grounded electrode. For the cylindrical and spherical models the inner electrode is driven; the outer electrode serves as the reference potential for the system, even when the inner electrode is not present. Equation (61) can be written at one-half grid cell from the boundary in conjunction with a central difference applied to the definition of potential to obtain:

planar

$$E_{1/2} = \frac{\Phi_0 - \Phi_1}{\Delta x} = \frac{1}{\varepsilon}\left(\sigma_+ + \rho_0 \frac{\Delta x}{2}\right) \tag{62}$$

cylindrical

$$E_{1/2} = \frac{\Phi_0 - \Phi_1}{\Delta r} = \frac{1}{\varepsilon}\left(\sigma_+ \frac{r_0}{r_{1/2}} + \frac{\rho_0}{2}\left(r_{1/2} - \frac{r_0^2}{r_{1/2}}\right)\right) \tag{63}$$

spherical

$$E_{1/2} = \frac{\Phi_0 - \Phi_1}{\Delta r} = \frac{1}{\varepsilon}\left(\sigma_+ \frac{r_0^2}{r_{1/2}^2} + \frac{\rho_0}{3}\left(r_{1/2} - \frac{r_0^3}{r_{1/2}^2}\right)\right). \tag{64}$$

Equations (57)–(59) and boundary conditions for the gridded system may be written in a general tridiagonal matrix form, to be evaluated at time t.

When the center conductor is not present in the curvilinear models the boundary conditions must be modified. From Gauss's Law the electric field at the origin must be zero. Integrating Gauss's Law from the origin to $r = r_{\frac{1}{2}}$, we obtain the modified form of (63) for the hollow cylindrical system [12, sec. 14-10]:

$$E_{1/2} = \frac{\Phi_0 - \Phi_1}{\Delta r} = \frac{1}{\varepsilon}\left(\frac{\rho_0}{2} r_{1/2}\right). \tag{65}$$

The particles are moved by obtaining E at each particle position using some weighting (in our case, the same used to weight particles), and applying this to Newton–Lorentz equation of motion.

The external circuit is coupled to (62)–(64) through conservation of charge at each wall:

$$A\,\Delta\sigma = Q_{\text{conv}} + \Delta Q \tag{66}$$

where Q_{conv} is the charge deposited by the convection (particle) current, and ΔQ is the charge deposited by the external circuit current, both over some interval in time. Equation (66) is applied at the positively biased electrode as shown in Figs. 14 and 15, guaranteeing conservation of charge at all times. The same logic can also be applied to the other electrode; however, the surface charge on the second electrode is determined readily from (46) when the first surface charge is known. The charge conservation equation becomes:

$$\sigma^t = \sigma^{t-\Delta t} + \frac{Q^t_{\text{conv}} + Q^t - Q^{t-\Delta t}}{A} \tag{67}$$

where Q is the charge on one plate of the external circuit capacitor. An alternate method of coupling the circuit to the potential matrix is applying the continuity of current (Kirchhoff's Current Law) at the boundary [12, sec. 16-9]:

$$\frac{\partial\sigma}{\partial t} = J_{\text{conv}} + \frac{I}{A} \tag{68}$$

where J_{conv} is the plasma convection current at the electrode. The methods are equivalent when a first-order backward difference is used for $\partial\sigma/\partial t$ and $I = \partial Q/\partial t$. Since Q_{conv} is in general a noisy quantity in a particle simulation, any other quantity in (66) and (68) will contain similar noise. Thus (66) causes the wall charge σ to be noisy, as might be expected, because the capacitor charge reacts to the particle convection current only through the wall charge; i.e., particles absorbed by the wall contribute immediately to σ, but the charge drains slowly to the capacitor through currents. It can be shown that (68) results in the convention current being absorbed gradually into σ, so the noise is induced in the capacitor charge Q (and consequently in the external current I) to satisfy conservation of charge. Therefore we use the conservation of charge method of (66).

For the general voltage-driven series RLC circuit, the capacitor charge Q is advanced using Kirchhoff's Voltage Law:

$$L\frac{d^2Q}{dt^2} + R\frac{dQ}{dt} + \frac{Q}{C} = V(t) + \Phi_{nc} - \Phi_0\,. \tag{69}$$

The polarity of the source and resultant positive current are shown in Figs. 14 and 15. The general circuit equation is finite differenced using the second-order backward Euler representation of the first derivative:

$$\frac{dQ^t}{dt} = \frac{3Q^t - 4Q^{t-\Delta t} + Q^{t-2\Delta t}}{2\Delta t} \tag{70}$$

and the second derivative:

$$\begin{aligned}\frac{d^2Q^t}{dt^2} &= \frac{3dQ^t/dt - 4dQ^{t-\Delta t}/dt + dQ^{t-2\Delta t}/dt}{2\Delta t} \\ &= \frac{9Q^t - 24Q^{t-\Delta t} + 22Q^{t-2\Delta t} - 8Q^{t-3\Delta t} + Q^{t-4\Delta t}}{4\Delta t^2}.\end{aligned} \tag{71}$$

The latter is obtained by a second application of the first derivative to Q.

The charge on the capacitor is not known at t. Combining (69)–(71), we obtain:

$$Q^t = \frac{V(t) + \Phi^t_{nc} - \Phi_0 - K}{\alpha_0} \tag{72}$$

where

$$K = \alpha_1 Q^{t-\Delta t} + \alpha_2 Q^{t-2\Delta t} + \alpha_3 Q^{t-3\Delta t} + \alpha_4 Q^{t-4Q^{t-4\Delta t}} \tag{73}$$

and the α's are functions of R, L, C, and Δt.

Combining the potential (Poisson) equation results with the circuit equation results (72) and (73), using the boundary condition (68), we obtain the self-consistent field solution matrix for the voltage-driven series RLC circuit case. The solution is then self-consistent and second-order accurate for the general circuit case. The matrix can be solved using any algorithm optimized for tridiagonal matrices.

We have explored the accuracy and stability of the finite-difference circuit equation in great detail, finding the second-order accuracy as expected and stability over a wide range of RC and L/R time constants. (Given in more detail by Verboncoeur *et al.* [89].)

IX. Addition of Monte Carlo Collisions to PIC Codes

PIC codes involve deterministic classical mechanics which generally move all particles simultaneously using the same time step. The only part left to chance is usually limited to choosing initial velocities and positions and injected velocities.

The objective is usually seeking collective effects due to self and applied fields. Some exceptions to uniform Δt's are the multiscale codes of Friedman *et al.* [42] (moving the slower particles less frequently than the faster particles, as well as allowing a nonuniform grid) and the electron subcycling of Adam *et al.* [1] (moving the electrons more frequently than the ions). In the orbit averaging of Cohen *et al.* [31], particles are all advanced at small time steps (good cyclotron orbits), but the fields are advanced less frequently, using averaged orbit data; as the calculations per particle are not reduced, the gain in speed comes in reducing the number of particles required as the averaged contribution of each particle can substitute for many particles handled conventionally.

On the other hand, MC codes are basically probabilistic in nature, seeking mostly collisional effects in relatively weak electric fields. For example, let a given charged particle be known by its (total) kinetic energy E and its velocity relative to some target particles. This information produces a collision frequency $\nu_{\text{coll}} = n_{\text{target}}\sigma(E)v_{\text{relative}}$ and a probability that a collision will occur. We may use this information in several ways.

We have already seen one way in the work of Burger [28], and a similar way in that of Shanny *et al.* [76].

Another way is in [50, chap. 10], in following the flow of electrons through a semiconductor lattice with many kinds of electron lattice collisions. (See also Boardman [15] for a similar exposition.) They assume a constant total scattering rate (independent of wavenumber) by adding a (dummy) self-scattering rate to the real rate, an invention attributed in [50] to Rees [74], [75]; we will come back to this. The time (between collisions) δt, considered that for free flight, is obtained by setting the cumulative probability (up to δt) equal to a random number and then inverting to obtain δt. The particle is then advanced over this δt, accelerated and displaced by the local $q(\boldsymbol{E} + \boldsymbol{v} \times \boldsymbol{B})$ forces. Then its velocity is scattered (dependent on the collision process). A typical picture is Fig. 16 from [50, p. 384], showing several scattering processes per field solution for the particle shown. Hockney and Eastwood [50, sec. 10-3-2] describe this procedure in great detail; for our plasma purposes, convert their wavenumber $\boldsymbol{k}$ to our velocity $\boldsymbol{v}$. They [50, sec. 10-3-3 and fig. 10-11] go on to describe modifying the normal particle mesh time stepping (at Δt) in order to incorporate scattering (at various δt's). They note [50, p. 383] a concern mentioned earlier in the introduction:

> During scattering we regard the ~ 8000 simulation particles as a sample from the distribution in the real device, whereas during the field calculation the particles are regarded as superparticles, so that they correctly apportion the total charge to the mesh. It is important to distinguish carefully the different roles played by the simulation particles during the different parts of the cycle.

This, of course, is very clearly a PIC–MCC code.

We now give yet another PIC–MCC approach, which has been developed in Berkeley[2] over the past three years for low-pressure, low-density plasmas, with only a few particles colliding per field time step Δt. Our range is roughly $p <$ few 100 mtorr, $n_e < 10^{10}/\text{cm}^3$, $T \approx$ few eV. Prior publications on this approach are by Boswell and Morey [19], Surendra *et al.* [79], [80], Vender and Boswell [87], and Vender [88]. So far, we have included electron collisions with neutrals (elastic scattering, excitation, and ionization) and ion collisions with neutrals (scattering and charge exchange), as well as electron and ion attachment for small particulates (radius $< \lambda_D$). Our method is to use only the time step of the PIC field solver and mover Δt and then to collide as many particles as is probable in that Δt separately, varying only their velocities, as shown in Fig. 17. This, of course, is very similar to the method of Burger [28], but with aspects of the Hockney and Eastwood approach for choosing the kind of collision to be done, and aspects of Shanny *et al.* [76] for doing the collisions in detail.

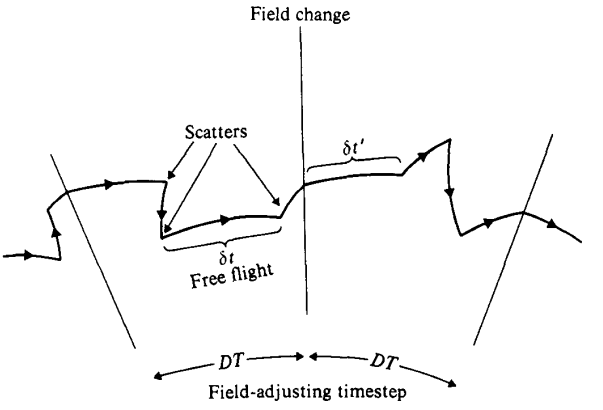

Fig. 16. A typical electron orbit for a high scattering rate, showing several free flights per field-adjusting time step. Scatters are indicated by a sharp change in the orbit. There is a slight change in the orbit every DT seconds due to the recalculation of the electric field (from Hockney and Eastwood [50]).

(Let us go through the method first, with the real scattering rates, then put in the dummy self-scattering or null collision method; we look at the physical reality first, then show how to shorten the numerical steps with the self/null methods.)

What quantities are we given? We have the local neutral gas properties (e.g., say, argon atoms at room temperature at p = 20 mtorr). We have approximations to cross sections for all of the collisions to be included, as a function of the charged-particle (total kinetic) energy E. Cross sections used for electrons are specified by $\sigma_{\max}$, E_0, E_1, E_2 as in Fig. 18, and for ions are specified by a, b, as in Fig. 19. We have all of the charged-particle velocities. Hence we know all of the collision frequencies between the charged particles and neutrals and the total $\nu_{\text{total}} = n_{\text{gas}}\sigma_{\text{total}}(E_m)v_m$; hence the probability of collision of the mth electron (or ion) in a time step Δt:

$$P_{\text{collision},\,m} = 1 - \exp[-n_{\text{gas}}\sigma_{\text{total}}(E_m)v_m\,\Delta t]. \qquad (74)$$

Here, e and i velocities v_m are taken to be much larger than those of gas atoms, so that $v_m - v_{\text{gas}} \cong v_m$ (this is good for electrons of course, but is not quite as good for the slow ions created by ionization or ions slowed to atom velocities by charge exchange). Note that we have slipped into treating our computer particles as single electrons, not as superparticles ($q_p = 10^8 e$); the implication is that with a sufficient number of collisions, the resultant scatter in energy and velocity will resemble that of the single particles.

The next step (as in Burger [28]) is to compare P_m with R_1, a uniform random number. For $P_m > R_1$, the particle m is to be

[2] Our Berkeley effort consists of my postdoctoral researcher I. Morey (who had begun collision work with R. Boswell at Australian National Univ., Canberra), M. Surendra (a student of Prof. D. Graves, Chem. Engr., Berkeley) and my students, V. Vahedi, J. Verboncoeur, and M. V. Alves.

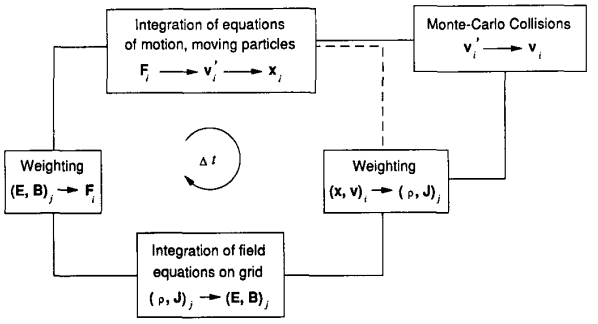

Fig. 17. Computing sequence for PIC–MIC with Monte Carlo collision velocity change made after the particle mover (from Alves *et al.* [3]).

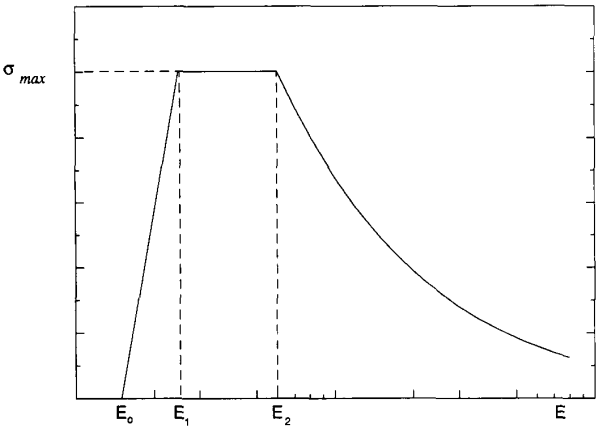

Fig. 18. Cross sections for electron–atom collisions specified by $\sigma_{\max}$ and energies E_0 , E_1 , E_2 . Decay $E > E_2$ is as $\ln E/E$.

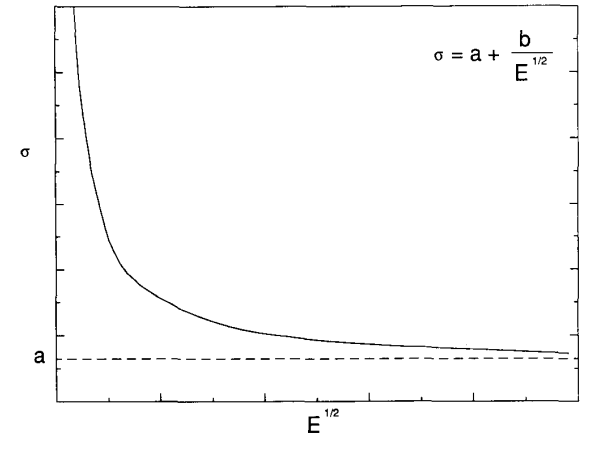

Fig. 19. Cross sections for ion–atom collisions specified by a and b, as shown.

scattered in the step Δt. For plasma parameters of interest to us, perhaps 5 particles in 1000 are to be scattered in Δt.

The next step is to determine which scattering process occurs. This is done (as in [50, fig. 10-9]) by assuming that the probability of process p is proportional to $\sigma_p(E_m)$ relative to $\sigma_{\text{total}}(E_m)$. We line up the relative cross sections 0 to 1, using markers $(\sigma_1)/\sigma_{\text{total}}$, $(\sigma_1 + \sigma_2)/\sigma_{\text{total}}$, $(\sigma_1 + \sigma_2 + \sigma_3)/\sigma_{\text{total}}$, up to 1; we choose the scattering process by where R_2 (uniform, random) falls.

The last step is to determine the new (scattered) velocity, and new particle velocities if ionization occurs. For such we need to look at each process separately. Elastic collisions change velocity angle of the scattered electrons; charge exchanges decrease ion energy and change velocity angle; ionizations do these and create an ion–electron pair, with new velocities. The effect on the neutral gas is *not* calculated. For example, excited atoms are assumed to have lifetimes less than the time step ($\sim 10^{-10}$ s) and do not lead to two-step ionization; hot atoms produced by charge exchange are ignored (but could be followed). Ionization by ions or hot atoms is not accounted for, because of relatively small cross sections.

Let us look first at electrons, determining the energy partitioning, and then determining the scattering angle.

For electron-neutral elastic collision, the atom is considered to have so large a mass that the electron only scatters in angle with no loss of energy.

For an electron-neutral excitation collision the energy of the scattered electron is simply:

$$E_{\text{scattered}} = E_{\text{incident}} - E_{\text{excitation}} \tag{75}$$

(e.g., for argon, $E_{\text{excitation}} = 11.55$ eV).

For an electron-neutral ionization collision the electron energies after the collision are equal to that before minus the ionization energy, or

$$E_{\text{scattered},\,e} + E_{\text{created},\,e} = E_{\text{incident},\,e} - E_{\text{ionization}}. \tag{76}$$

We have neglected the (small) energies of the created ion and the neutral; in fact, the created ion is given the energy associated with the neutral, so such neglect cancels. The energy is divided between the two electrons by treating the differential cross section as a distribution function, and inverting it. We use a simplified form of the differential cross section of Opal *et al.* [69]; setting the cumulative value of this cross section (integrated over incident energy, up to $E_{\text{incident},\,e}$) equal to a random number R_3 produces:

$$E_{\text{scattered},\,e} = B \tan\left[R_3 \tan^{-1}\left(\frac{E_{\text{incident},\,e} - E_{\text{ionization}}}{2B}\right)\right] \tag{77}$$

where B is known (e.g., for argon, $B \cong 10$ eV over our range of interest). The energy of the electron created is now simply:

$$E_{\text{created},\,e} = E_{\text{incident},\,e} - E_{\text{ionization}} - E_{\text{scattered},\,e}. \tag{78}$$

Now we have the energies (speeds) of the scattered particles; we need to find the scattering angle (new velocity components). Let the incident velocity (vectors) be v and the scattered be v' as shown in Fig. 20. We are calculating the angle χ; the angle ϕ is random over 2π, chosen by $2\pi R_4$ (R_4 is a uniform random number). We do this again by inverting the differential cross section as given in Surendra *et al.* [79]:

$$\frac{\sigma(E,\chi)}{\sigma(E)} = \frac{E}{4\pi\left(1 + E\sin^2\chi/2\right)\ln(1+E)} \tag{79}$$

where E is $E_{\text{scattered}}$ in eV (analytic fit for He, Ar). The angle χ is found by setting the cumulative distribution function equal to

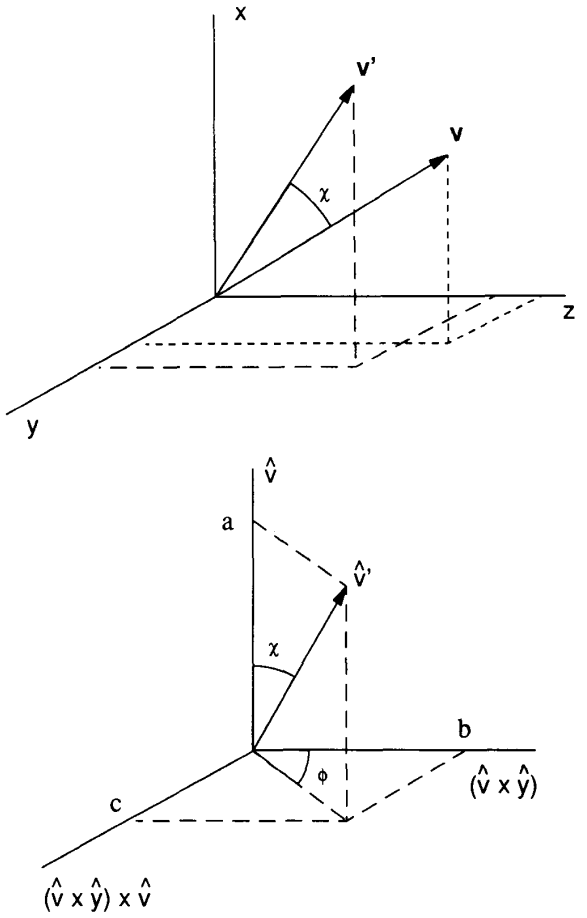

Fig. 20. Coordinates in configuration and velocity space for jump from v' to v.

a uniform random number R_4:

$$R_4 = \frac{2\pi}{\sigma(E)} \int_0^{\chi} \sigma(E, \chi') \sin \chi' d\chi' \tag{80}$$

and solving for χ. For the form given, there is an analytic solution (E in eV):

$$\cos \chi = \frac{2 + E - 2(1+E)^{R_4}}{E} \tag{81}$$

where E is $E_{\text{scattered}}$. Note that for large E, $\cos \chi \to 1$, $\chi \to 0$, forward scattering; for small E, $\cos \chi \to 1 - 2R_4$, uniform -1 to $+1$, which (one may show) is isotropic in χ, 0 to π.

Let us now look at the ion scattering. The ion collision cross sections are specified simply by:

$$\sigma = a + b/\sqrt{E} \tag{82}$$

with a and b given separately for elastic and charge exchange. (Note that $\sigma v \sim b$ for $E \to 0$, no singularity in σv as $E \to 0$.) Let the choice between elastic scattering and charge exchange be made as before. The colliding ions and atoms have (essentially) the same mass (e.g., Ar^+ and Ar).

For elastic scattering (hard sphere, equal masses) we use:

$$E_{\text{scattered},\,i} = E_{\text{incident},\,i} \cos^2 \chi \tag{83}$$

where $\cos^2 \chi = 1 - \sin^2 \chi$; $\sin^2 \chi = \frac{1}{2}(1 - \cos 2\chi)$, where $2\chi = \Theta$, the center of mass scattering angle. χ is obtained from:

$$\cos \Theta = \cos 2\chi = 1 - 2R_5 \quad (\text{uniform } -1 \text{ to } 1),$$
$$\cos \chi = \sqrt{1 - R_5} \tag{84}$$

isotropic scatter, χ up to $\pi/2$. The scatter in ϕ is uniform 0 to $2\pi(\phi = R_6 2\pi)$.

For charge exchange, the incident fast ion picks up an electron from a slow gas atom (becoming a fast atom) and leaving behind a slow scattered ion. The particles exchange forward momentum. The slow ion is scattered isotropically; χ is uniform 0 to $\pi(R_7 \pi)$ and ϕ is chosen as always, uniform 0 to $2\pi(R_8 2\pi)$. The speed of the scattered ion is chosen to match the gas atom velocity distribution (Gaussian) by inverting the cumulative velocity distribution in $3v$, numerically.

This concludes the collision calculations. There is much more atomic physics yet to be incorporated, such as assigning more "quality" to the superparticles, charged and neutral, and following the neutrals.

Finally, let us describe the numerically efficient self-scattering process noted earlier due to Rees [74], [75], also called the null-collision method due to Boeuf and Marode [16], and Lin and Bardsley [58]. Construct a fake cross section, $\sigma_{\text{fake}} > \sigma_{\text{total}}$ for all energies E, and $\sigma_{\text{fake}} \sim 1/v$, making $\nu_{\text{coll}} = n_{\text{gas}}(\sigma_{\text{fake}} v)$ independent of energy. Hence we need *not* calculate $\sigma(E)$ for every particle and every time step, which is a great savings. For our PIC–MCC approach, we use $P = 1 - \exp(-\nu_{\text{coll}} \Delta t) = R_1$ to give us the fraction of particles to be collided in Δt. These particles (with uniform ν_{coll}) are simply chosen randomly from the whole set (say, from all electrons, with care not to pick the same electron twice). Which collision process takes place is again chosen proportional to $\Delta\sigma/\sigma_{\text{total}}$; however, when R_2 lands on σ_{fake}, the collision is skipped. In this manner $\sigma(E_m)$ is needed only for the particles colliding. Our current PIC plus MCC 1-D3v plasma device codes run about half the speed of PIC alone. We expect a saving of 10 to 20% in running time by going to the self-scattering or null-collision method.

X. Discussion

PIC and MCC plasma simulations have existed separately for several decades, with PIC applied primarily to hot fully ionized collisionless plasmas (especially to fusion plasmas), and MCC applied to cool weakly ionized gases (especially to laboratory discharges). Early workers in the 1960's showed the way to meld these two simulation techniques, but without leading to many new applications. However, in the past decade the interest has grown in understanding plasma behavior with bounding walls emitting or absorbing, grounded, biased, or RF driven, with a wide range of applications. As a result, the early melding of PIC and MCC has now grown to many efforts. The hope in this paper has been to display the transition from early electrostatic many-sheet Gauss's Law models to particle-mesh (PIC) models, with some mention of enhancing collisions (such as particle–particle–particle-mesh). Some PIC simulation theory was given to show that (and how) such can be done and, as an example, to present the result that even a Maxwellian velocity distribution can be (mildly) unstable for $\lambda_D/\Delta x \lesssim 0.3$; there are many other results, the sum total being a rather well-developed PIC simulation science. MCC simulations have had wide application to both collisional plasmas and to electron flow in semiconductors, with many publications. What is displayed here is our method of melding PIC with MCC, which we (and

others) are still developing. As yet, our base for verifying our PIC–MCC simulation methods is small relative to decades both of collisionless PIC work and collisional MCC work, but is expanding. PIC–MCC simulations here and elsewhere appear to read well against other approaches (analytic models, fluid simulations, laboratory experiments.) Our own PIC–MCC applications have been in 1-D3v to RF discharges, magnetized and not, symmetric and asymmetric [3] and to plasma-immersion ion implantation [86]. An example of our bounded magnetized work with fusion plasma in 2-D3v is [83], [84]. There is no room to show these applications here; good examples are in [87] and [80].

A last word: We have done our code development on fast PC's in a highly interactive mode viewed in real time, with literally dozens of diagnostics, looking for real laboratory values. Some problems run in minutes, others in hours; typically the PC processes 5000 particles/s. Workstations increase this speed to a few 100 000 particles/s, again with real-time viewing. Supercomputers, of course, increase the speed by 10 or more; the step to massively paralleled computers buys more orders of magnitude in speed. We advocate using the whole chain (PC–WS–SC–MPC) when possible as a direct solution of whole device plasma problems, as complementary to analytic modeling and laboratory experiments, for everyday use by theorists, simulators, and experimentalists.

Acknowledgment

Many people have contributed to the developments presented here, starting with the pioneering works of D. R. Hartree, P. K. Tien, and O. Buneman in the 1950's, and J. M. Dawson, R. W. Hockney, P. Burger, R. Shanny, R. L. Morse, and C. W. Nelson in the 1960's. I wish I could list *all* of my students and postdoctoral researchers who have taught me much and worked very hard, starting with W. B. Bridges in 1959, and especially A. B. Langdon, whose simulation theory is a real cornerstone. Our bounded plasma work began with electron diodes in 1959; our whole-plasma device work began in earnest in 1981, initially for fusion walls, limiters, and diverters. PDW1 was written in 1983 by W. S. Lawson, with help from T. L. Crystal, P. Gray, and S. Kuhn, now widely applied. Our more recent interactive computer experiments, full PIC–MCC for partially ionized plasmas, were developed by V. Vahedi, J. Verboncoeur, I. J. Morey, M. V. Alves, and F. Tsung, with profitable discussions with M. Surendra and R. Porteous (who work with Prof. D. B. Graves), and with R. Boswell and D. Vender of ANU, Canberra. Especially helpful have been guidelines provided by the analytic models of Prof. M. A. Lieberman, and interactions with him and his experimental students.

References

[1] J. C. Adam, A. Gourdin Serveniere, and A. B. Langdon, "Electron sub-cycling in particle simulation of plasmas," *J. Comput. Phys.,* vol. 47, pp. 229–244, Aug. 1982b.

[2] B. Alder, S. Fernbach, and M. Rotenberg, Eds., *Plasma Physics* (Meth. Comput. Phys, vol. 9). New York: Academic, 1970; see also, *Plasma Physics* (Meth. Comput. Phys., vol. 16). New York: Academic, 1976.

[3] M. V. Alves, M. A. Lieberman, V. Vahedi, and C. K. Birdsall, "Sheath voltage ratio for asymmetric RF discharges," *J. Appl. Phys.,* to be published.

[4] P. L. Auer, H. Hurwitz, and R. W. Kilb, "Low Mach number magnetic compression waves in a collision-free plasma," *Phys. Fluids,* vol. 4, pp. 1105–1121, Sept. 1961.

[5] P. L. Auer, H. Hurwitz, and R. W. Kilb, "Large-amplitude magnetic compression of a collision-free plasma, II. Development of a thermalized plasma," *Phys. Fluids,* vol. 5, pp. 298–316, Mar. 1962.

[6] C. K. Birdsall and W. B. Bridges, "Space-charge instabilities in electron diodes and plasma converters," *J. Appl. Phys.,* vol. 32, pp. 2611–2618, 1961; see also, W. B. Bridges, and C. K. Birdsall, "Space-charge instabilities in electron diodes II," *J. Appl. Phys.,* vol. 34, pp. 2946–2955, 1963.

[7] C. K. Birdsall and W. B. Bridges, *Electron Dynamics of Diode Regions.* New York: Academic, 1966.

[8] C. K. Birdsall and D. Fuss, " Cloud-in-cell computer experiments in two and three dimensions," in *Proc. 2nd Conf. Num. Sim. Plasmas* (Los Alamos, NM), Sept. 1968.

[9] C. K. Birdsall, A. B. Langdon, C. F. McKee, H. Okuda, and D. Wong, "Theory and experiments for a plasma consisting of clouds interacting with clouds (CIC) with and without a spatial grid," in *Proc. 2nd Conf. Num. Sim. Plasmas* (Los Alamos, NM), Sept. 1968.

[10] C. K. Birdsall and D. Fuss, "Clouds-in-clouds, clouds-in-cells physics for many-body simulation," *J. Comput. Phys.,* vol. 3, pp. 494–511, Apr. 1969.

[11] C. K. Birdsall and J. M. Dawson, "Plasma physics," in *Computers and their Role in the Physical Sciences,* S. Fernbach and A. Taub, Eds. New York: Academic, 1970, pp. 247–310.

[12] C. K. Birdsall and A. B. Langdon, *Plasma Physics Via Computer Simulation.* New York: McGraw-Hill, 1985.

[13] C. K. Birdsall, A. B. Langdon, and H. Okuda, "Finite-size particle physics applied to plasma simulation," *Plasma Physics* (Methods Comput. Phys., vol. 9). New York: Academic, 1970, pp. 241–258.

[14] J. U. Blackbill and B. I. Cohen, Eds., *Multiple Times Scales.* New York: Academic, 1985.

[15] A. D. Boardman, "Computer simulation of hot electron behavior in semiconductors using Monte Carlo methods," in *Applied Physics* (Phys. Prog., vol. 4). New York: Wiley, 1980, pp. 355–410.

[16] J. P. Boeuf and E. Marode, "A Monte Carlo analysis of an electron swarm in a nonuniform field: The cathode region of a glow discharge in helium," *J. Phys. D,* vol. 15, pp. 2169–2187, 1982.

[17] J. P. Boris and K. V. Roberts, "Optimization of particle calculations in 2 and 3 dimensions," *J. Comput. Phys.,* vol. 4, pp. 552–571, Dec. 1969.

[18] J. P. Boris, "Relativistic plasma simulation-optimization of a hybrid code," in *Proc. 4th Conf. Num. Sim. Plasmas* (Washington, DC), Nov. 1970, pp. 3–67.

[19] R. Boswell and I. J. Morey, "Self-consistent simulation of a parallel-plate RF discharge," *Appl. Phys. Lett.,* vol. 52, pp. 21–23, Jan. 1988.

[20] O. Buneman, "Dissipation of currents in ionized media," *Phys. Rev.,* vol. 115, pp. 503–517, Aug. 1959.

[21] O. Buneman, "Time reversible difference procedures," *J. Comput. Phys.,* vol. 1, pp. 517–535, June 1967.

[22] O. Buneman, "Fast numerical procedures for computer experiments on relativistic plasmas," in *Relativistic Plasmas,* O. Buneman and W. Pardo, Eds. New York: Benjamin, 1968, pp. 205–219.

[23] O. Buneman and D. Dunn, "Computer experiments in plasma physics," *Science J.,* vol. 2, pp. 34–43, July 1966.

[24] P. Burger, "Nonexistence of dc states in low-pressure thermionic converters," *J. Appl. Phys.,* vol. 35, pp. 3048–3049, 1964.

[25] P. Burger, "The opposite-stream plasma diode," Ph.D. thesis, Stanford Univ., Palo Alto, CA, 1964.

[26] P. Burger, "Theory of large-amplitude oscillation in the one-dimensional low-pressure cesium thermionic converter," *J. Appl. Phys.,* vol. 36, pp. 1938–1943, 1965.

[27] P. Burger, D. A. Dunn, and A. S. Halstead, "Computer experiments on the randomization of electrons in a collisionless plasma," *Phys. Fluids,* vol. 8, pp. 2263–2272, 1965.

[28] P. Burger, "Elastic collisions in simulating one-dimensional plasma diodes on the computer," *Phys. Fluids,* vol. 10, pp. 658–666, 1967.

[29] L. Chen and C. K. Birdsall, "Heating of magnetized plasmas by a large-amplitude low-frequency electric field," *Phys. Fluids,* vol. 16, pp. 2229–2240, Dec. 1973.

[30] C. D. Child, "Discharge from hot CaO," *Phys. Rev.,* ser. I, vol. 32, pp. 492–511, 1911

[31] B. I. Cohen, T. A. Brengle, D. B. Conley, and R. P. Freis, "An orbit-averaged particle code," *J. Comput. Phys.,* vol. 38, pp. 45–63, Nov. 1980.

[32] B. I. Cohen and R. P. Freis, "Stability and application of an orbit-averaged magnetoinductive particle code," *J. Comput. Phys.,* vol. 45, pp. 367–373, Mar. 1982.

[33] J. M. Dawson, "One-dimensional plasma model," *Phys. Fluids,* vol. 5, pp. 445–459, Apr. 1962.

[34] J. M. Dawson, "Particle simulation of plasmas," *Rev. Mod. Phys.*, vol. 55, pp. 403–447, Apr. 1983.
[35] J. M. Dawson and C. Smith, "Some investigations of plasma instabilities in one-dimensional plasmas," Princeton Plasma Phys. Lab., Tech. Rep. MATT-152, 1962.
[36] J. Denavit and W. L. Kruer, "How to get started in particle simulation," *Plasma Phys. Control. Fusion,* vol. 6, pp. 35–44, Apr. 1980.
[37] D. A. Dunn and I. T. Ho, "Computer experiments on ion-beam neutralization with initially cold electrons," Stanford Electron. Res. Lab., Palo Alto, CA, Tech. Rep. SEL-73-046, Apr. 1963; see also, D.A. Dunn, *Models of Particles and Moving Media.* New York: Academic, 1971.
[38] J. W. Eastwood, R. W. Hockney, and D. N. Lawrence, "P3M3DP—the three-dimensioal periodic particle/particle-mesh program," *Comput. Phys. Commun,.* vol. 19, pp. 215–261, 1980.
[39] O. C. Eldridge and M. Feix, "One-dimensional plasma model at thermodynamic equilibrium," *Phys. Fluids,* vol. 5, pp. 1076–1080, 1962.
[40] O. C. Eldridge and M. Feix, "Numerical experiments with a plasma model," *Phys. Fluids,* vol. 6, pp. 398–406, Mar. 1963.
[41] B. D. Fried and S. D. Conte, *Plasma Dispersion Function.* New York: Academic, 1961.
[42] A. Friedman, S. E. Parker, S. L. Ray, and C. K. Birdsall, "Multi-scale particle in cell plasma simulation," *J. Comput. Phys.*, to be published.
[43] T. C. Fry, "The thermionic current between parallel-plane electrodes: Velocities distributed according to Maxwell's law," *Phys. Rev.*, vol. 17, p. 441, Apr. 1921.
[44] F. H. Harlow, "The particle-in-cell computing method for fluid dynamics," in (Meth. Comput. Phys.,vol. 3), B. Alder, S. Fernbach, and M. Rotenberg, Eds. New York: Academic, 1964.
[45] D. R. Hartree, "Some calculations of transients in an electronic valve," *Appl. Sci. Res.*, vol. B1, pp. 379–390, 1950.
[46] A. Hasegawa and C. K. Birdsall, "Sheet-current plasma model for ion-cyclotron waves," *Phys. Fluids,* vol. 7, pp. 1590–1600, Oct. 1964.
[47] R. W. Hockney, Electron Dev. Lab., Stanford Electron. Lab., Stanford, CA, Quart. Res. Rev. No. 4, p. I-102, 1 Jan.–31 Mar. 1963.
[48] R. W. Hockney, "A fast direct solution of Poisson's equation using Fourier analysis," *J. Assoc. Comput. Mach.,* vol. 12, pp. 95–113, Jan. 1965.
[49] R. W. Hockney, "Computer simulation of anomalous plasma diffusion and numerical solution of Poisson's equation," *Phys. Fluids,* vol. 9, pp. 1826–1835, Sept. 1966; see also, R.W. Hockney, "Characteristics of noise in a 2–D computer plasma," *Phys. Fluids*, vol. 11, pp. 1381–1383, June 1968; R.W. Hockney, "The potential calculation and some applications," in *Plasma Physics* (Meth. Comput. Phys., vol. 9), B. Alder, S. Fernbach, and M. Rotenberg, Eds. New York: Academic, 1970, pp. 135–211.
[50] R. W. Hockney and J. W. Eastwood, *Computer Simulation Using Particles.* New York: McGraw-Hill, 1981.
[51] A. B. Langdon, "Nonphysical modifications to oscillations, fluctuations, and collisions due to space-time differencing," in *Proc. 4th Conf. Num. Sim. Plasmas* (Washington, DC), Nov. 1970, pp. 467–495.
[52] A. B. Langdon, "Effect of the spatial grid in simulation plasmas," *J. Comput. Phys.,* vol. 6, pp. 247–267, Oct. 1970.
[53] A. B. Langdon, "Kinetic theory of fluctuations and noise in computer simulation of plasma," *Phys. Fluids,* vol. 22, pp. 163–171, Jan. 1979.
[54] A. B. Langdon and J. M. Dawson, "Investigations of a sheet model for a bounded plasma field and radiation," in *Proc. 1st Conf. Num. Sim. Plasmas* (Williamsburg, VA), Apr. 1967, pp. 39–40.
[55] A. B. Langdon and C. K. Birdsall, "Theory of plasma simulation using finite-size particles," *Phys. Fluids,* vol. 13, pp. 2115–2122, Aug. 1970.
[56] A. B. Langdon and B. F. Lasinski, "Electromagnetic and relativistic plasma simulation models," in *Meth. Comput. Phys.,* vol. 16, B. Alder, S. Fernbach, M. Rotenberg, and J. Killeen, Eds. New York: Academic, 1976, pp. 327–366.
[57] I. Langmuir, "The effect of space charge and initial velocities on the potential distribution and thermionic current between parallel electrodes," *Phys. Rev.,* vol. 21, pp. 419–435, Apr. 1923.
[58] S. L. Lin and J. N. Bardsley, "Monte Carlo simulations of ion motion in drift tubes," *J. Chem. Phys.,* vol. 66, pp. 435–445, 1977.
[59] E. L. Lindman, "Dispersion relation for computer-simulated plasmas," *J. Comput. Phys.,* vol. 5, pp. 13–22, Feb. 1970.
[60] R. J. Lomax, "Transient space-charge flow," *J. Electron. Contr.,* vol. 9, pp. 127–140, 1960.
[61] Y. Matsuda and H. Okuda, "Collisions in multi-dimensional plasma simulations," *Phys. Fluids,* vol. 18, pp. 1740–1747, Dec. 1975.
[62] D. Montgomery and C. W. Neilson, "Thermal relaxation in one- and two-dimensional plasma models," *Phys. Fluids,* vol. 13, pp. 1405–1407, May 1970.
[63] R. L. Morse and C. W. Neilson, "Numerical simulation of a warm two-beam plasma," in *Proc. 2nd Conf. Num. Sim. Plasmas* (Los Alamos, NM), Sept. 1968.
[64] R. L. Morse and C. W. Neilson, "Numerical simulation of warm two-beam plasma," *Phys. Fluids,* vol. 12, pp. 2418–2425, Nov. 1969.
[65] R. L. Morse and C. W. Neilson, "Numerical simulation of the Weibel instability in one and two dimensions," *Phys. Fluids,* vol. 14, pp. 830–840, Apr. 1971.
[66] H. Okuda, "Verification of theory for plasma of finite-size particles," *Phys. Fluids,* vol. 15, pp. 1268–1274, July 1972.
[67] H. Okuda, "Nonphysical noises and instabilities in plasma simulation due to a spatial grid," *J. Comput. Phys.,* vol. 10, pp. 475–486, Dec. 1972.
[68] H. Okuda and C. K. Birdsall, "Collisions in a plasma of finite-size particles," *Phys. Fluids,* vol. 8, pp. 2123–2134, Aug. 1970.
[69] C. B. Opal, W. K. Peterson, and E. C. Beaty, Jr., "Measurements of secondary electron spectra produced by electron impact ionization of a number of simple gases," *J. Chem. Phys.,* vol. 55, pp. 4100–4106, 1971.
[70] D. Potter, *An Introduction to Computational Physics.* London: Wiley, 1973.
[71] R. J. Procassini, C. K. Birdsall, E. C. Morse, and B. I. Cohen, "A relativistic Monte Carlo binary collision model for use in plasma particle simulation codes," Univ. California, Berkeley, Memo. UCB/ERL M87/24, 14 May 1987.
[72] R. J. Procassini and B. I. Cohen, "The TESS computer code user's manual," Lawrence Livermore Nat. Lab., Livermore, CA, UCRL-ID-104092, June 18, 1990.
[73] R. J. Procassini and B. I. Cohen, "The DIPSI computer code user's manual," Lawrence Livermore Nat. Lab., Livermore, CA, UCRL-ID-104093, June 18, 1990.
[74] H. D. Rees, "Calculation of steady-state distribution function by exploiting stability," *Phys. Lett.,* vol. 26A, pp. 416–417, 1968.
[75] H. D. Rees, "Calculation of distribution functions by exploiting the stability of the steady state," *J. Phys. Chem. Solids,* vol. 30, pp. 643–655, 1969.
[76] R. Shanny, J. M. Dawson, and J. M. Greene, "One-dimensional model of a Lorentz plasma," *Phys. Fluids,* vol. 10, pp. 1281–1287, June 1967.
[77] L. Spitzer, Jr., *Physics of Fully Ionized Gases,* 2nd ed. New York: Wiley-Interscience, 1962.
[78] M. Surendra, D. B. Graves, and I. J. Morey, "Electron heating in low pressure RF glow discharges," *Appl. Phys. Lett.,* vol. 56, pp. 1022–1024, 12 Mar. 1990.
[79] M. Surendra, D. B. Graves, and G. M. Jellum, "Self-consistent model of a direct-current glow discharge: Treatment of fast electrons," *Phys. Rev. A,* vol. 41, pp. 1112–1125, 15 Jan. 1990.
[80] M. Surendra and D. B. Graves, "Particle simulations of radiofrequency glow discharges," *IEEE Trans. Plasma Sci.*, this issue.
[81] T. Takizuka and H. Abe, "A binary collision model for plasma simulation with a particle code," *J. Comput. Phys.,* vol. 25, pp. 205–219, 1977.
[82] T. Tajima, *Computational Plasma Physics, With Applications to Fusion and Astrophysics.* Reading, MA: Addison-Wesley, 1989.
[83] K. Theilhaber and C. K. Birdsall, "Kelvin–Helmholtz vortex formation and particle transport in a cross-field sheath I: Transient behavior," *Phys. Fluids B,* vol. 1, pp. 2244–2259, Nov. 1989.
[84] K. Theilhaber and C. K. Birdsall, "Kelvin–Hemholtz vortex formation and particle transport in a cross-field sheath II: Steady state," *Phys. Fluids B,* vol. 1, pp. 2260–2272, Nov. 1989.
[85] P. K. Tien and J. Moshman, "Monte Carlo calculation of noise near the potential minimum of a high-frequency diode," *J. Appl. Phys.,* vol. 27, pp. 1067–1078, 1956.
[86] V. Vahedi, M. A. Lieberman, M. V. Alves, J. P. Verboncoeur, and C. K. Birdsall, "A one-dimensional collisional model for plasma immersion ion implantation," *J. Appl. Phys.,* to be published.

[87] D. Vender and R. W. Boswell, "Numerical modeling of low pressure RF plasmas," *IEEE Trans. Plasma Sci.*, vol. 18, pp. 725–732, Aug. 1990.
[88] D. Vender, "Numerical studies of the low pressure RF plasma," Ph.D. thesis, Australian Nat. Univ., Canberra, Sept. 1990.
[89] J. Verboncoeur, M. V. Alves, and V. Vahedi, "Simultaneous potential and circuit solution for bounded plasma particle simulation codes," Electron. Res. Lab. Tech. Memo. No. UCB/ERL M90/67, Aug. 7, 1990.
[90] R. P. Wadhwa, O. Buneman, and D. F. Brauch, "Two-dimensional computer experiments on ion-beam neutralization," *Amer. Inst. Aeronaut. Astonaut.*, vol. 3, pp. 1976–1981, 1965.
[91] S. P. Yu, G. P. Kooyers, and O. Buneman, "A time-dependent computer analysis of electron-wave interaction in crossed-fields," *J. Appl. Phys.*, vol. 36, pp. 2550–2559, Aug. 1965.

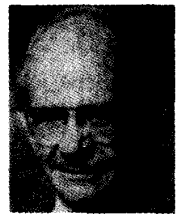

C. K. Birdsall (S'47–A'51–M'56–SM'59–F'62) received the B.S.E. and M.S.E. degrees from the University of Michigan, Ann Arbor, and the Ph.D. degree from Stanford University, Palo Alto, CA (1951).

From 1951–1955 he worked at the Hughes Aircraft Company on microwave tubes, including resistive-wall, reactive-wall, and rippled-wall amplifiers, as well as on periodic structures (e.g., ring-bar helix) and large-C analysis for high-power traveling tubes, leading to the first multikilowatt TWT at X-band. From 1955–1959 he was at the General Electric Microwave Laboratory as Leader of the Electron Physics Group, where he worked on electron guns, streams, and traveling-wave tubes. In 1959 he joined the Electrical Engineering Department, University of California, Berkeley. An early result was the discovery of virtual cathode oscillations using computer simulations with W. B. Bridges; they co-authored the book, *Electron Dynamics of Diode Regions* (1966). His research moved to high-temperature plasmas, with an emphasis on understanding instabilities, heating, and transport through the development and application of many-particle computer simulations. He founded the Plasma Theory and Simulation Research Group in 1967 with A. B. Langdon; they later co-authored the book, *Plasma Physics Via Computer Simulation* (1985). During 1972–1974 he founded and chaired the campus-wide Energy and Resources Program (now ERG), with faculty, integrative courses at all levels, and interdisciplinary research. During 1981–1982 he began the study of plasma–surface interactions.

Dr. Birdsall is a Fellow of the APS and AAAS and was the first recipient (1988) of the IEEE Plasma Science and Applications Award.